REPUBLIC OF TÜRKİYE
ERCIYES UNIVERSITY
THE GRADUATE SCHOOL OF NATURAL AND APPLIED SCIENCES
THE DEPARTMENT OF NANOSCIENCE AND NANOTECHNOLOGY

DESIGN AND SYNTHESIS OF COUMARIN-BASED FLUORESCENT MOLECULES FOR PHOTODYNAMIC THERAPY OF CANCEROUS CELLS

Prepared by
Abdul REHMAN

Advisor
Assoc. Prof. Dr. Yavuz Nuri ERTAŞ

Master of Science Thesis

August 2024
KAYSERİ

REPUBLIC OF TÜRKİYE
ERCIYES UNIVERSITY
THE GRADUATE SCHOOL OF NATURAL AND APPLIED SCIENCES
THE DEPARTMENT OF NANOSCIENCE AND NANOTECHNOLOGY

DESIGN AND SYNTHESIS OF COUMARIN-BASED FLUORESCENT MOLECULES FOR PHOTODYNAMIC THERAPY OF CANCEROUS CELLS

Prepared by
Abdul REHMAN

Advisor
Assoc. Prof. Dr. Yavuz Nuri ERTAŞ

The current study was funded by Erciyes University Scientific Research Projects Unit under the code of FYL-2023-13390

August 2024
KAYSERİ

COMPLIANCE WITH SCIENTIFIC ETHICS

I hereby confirm that all the information provided in this work was collected and put forward in accordance with ethical standards and academic guidelines. I also declare that I correctly cited and referenced any source material and findings that are not original to my work, as required by these regulations and conduct. I declare that this work is the result of my own study and has not been submitted anywhere else for a degree. Each information source that has been evaluated follows academic ethics and has been properly assigned.

Abdul Rehman

Signature

The Master of Science thesis entitled **"Design and Synthesis of Coumarin-Based Fluorescent Molecules for Photodynamic Therapy of Cancerous Cells"** has been prepared following Erciyes University Graduate School of Natural and Applied Sciences Thesis Preparation and Writing Guide.

Prepared by
Abdul REHMAN

Advisor
Assoc. Prof. Yavuz Nuri ERTAŞ

Head of The Department of Nanoscience and Nanotechnology

Prof. Dr. Mustafa Serdar ÖNSES

ACKNOWLEDGMENT

First and foremost, I would like to express my deepest gratitude to my supervisor, **Assoc. Prof. Yavuz Nuri ERTAŞ** for his invaluable guidance, continuous support, and encouragement throughout my research.

Special thanks go to my colleague **Elif LÜLEK** at Ertas Lab, Nanotechnology Application and Research Center. I am particularly grateful to **Dr. Sayed Mir SAYED** for his assistance and support in various aspects of my research. Their collaboration, camaraderie, and constant willingness to help made this journey a memorable and fulfilling experience.

I would like to extend my sincere appreciation to the funding agencies, TÜBİTAK-2232/B International Fellowship for Early-Stage Researchers (Project No. 121C157) and Scientific Research Projects Unit (BAP) Institute of sciences Erciyes University **(**Project No. FYL-2023-13390) for their financial support, as without their support this work would not have been possible.

Finally, I would like to thank my parents (**Mr. Waris Ali KHAN / Mrs. SHAZIA**), my brothers (**Majid IQBAL, Muhammad Usman, Muhammad Imran**), and my sister (**Tehreem SHAHZADI)** for their unwavering support and understanding throughout my academic journey. Their love and encouragement have been my greatest source of strength.

This thesis is dedicated to all those who believed in me and supported me in my pursuit of knowledge.

Abdul Rehman

August 2024, KAYSERİ

DESIGN AND SYNTHESIS OF COUMARIN-BASED FLUORESCENT MOLECULES FOR PHOTODYNAMIC THERAPY OF CANCEROUS CELLS

Abdul REHMAN

Erciyes University, Graduate School of Natural and Applied Sciences
Master of Science Thesis, August 2024
Advisor: Assoc. Prof. Yavuz Nuri ERTAŞ

ABSTRACT

Organic fluorescent molecules play a great role in biomedical sciences, particularly in biosensing, imaging, and theranostics. Inspired by the wide-spread use of organic fluorescent molecules as Photosensitizers, herein two novel coumarin based fluorescent molecules named TPAV-CM-Py-Me and TPAV-CM-Py with aggregation induced emission phenomenon that is highly desirable in biomedical sciences were synthesized. Both AIEgens have absorbance maxima in the visible region (beyond 400 nm) and can be readily excited through the ordinary white light to be used in cancer treatment. To confirm that the designed AIEgens can produce reactive oxygen species (ROS), 9,10-anthracenediyl-bis(methylene)-dimalonic acid (ABD commercial sensor) was used for singlet oxygen sensing, and it was found that both AIEgens have the ability to generate ROS under white light irradiation. The intracellular ROS generation was investigated via confocal microscopy using DCFH-DA dye and it was found that the molecules can generate intracellular ROS under white light irradiation. Both molecules have a strong affinity for mammalian cells and can easily stain the plasma membrane. Inspired by the high ROS generation and strong affinity toward mammalian cells, they were used against MCF-*7* breast cancer cells, and it was found that both AIEgens can kill the cancer cells under white light irradiation. The sizes of the nanoaggregates were studied via dynamic light scattering and scanning electron microscopy. Inspired by their effective use against cancer cells, the designed molecules may find potential practical applications in photodynamic treatment of cancer.

Keywords: Fluorescent Molecules, Aggregation Induced Emission, Photosensitizers, Cell Imaging, Photodynamic Therapy

DESIGN AND SYNTHESIS OF COUMARIN-BASED FLUORESCENT MOLECULES FOR PHOTODYNAMIC THERAPY OF CANCEROUS CELLS

Abdul REHMAN

Erciyes Üniversitesi, Fen Bilimleri Enstitüsü
Yüksek Lisans Tezi, Ağustos 2024
Danışman: Doç. Dr. Yavuz Nuri ERTAŞ

ÖZET

Organik floresan moleküller, biyomedikal bilimler başta olmak üzere biyoalgılama, görüntüleme ve teranostik alanlarında büyük rol oynamaktadır. Organik floresan moleküllerin, fotosensitizör olarak yaygın kullanımından esinlenerek biyomedikal biliminde oldukça arzu edilen agregasyon kaynaklı emisyon fenomenine sahip TPAV-CM-Py-Me ve TPAV-CM-Py adlı iki yeni kumarin bazlı floresan molekülünün sentezini rapor ediyoruz. Her iki AIEjeni de görünür bölgede (>400 nm) maksimum absorpsiyona sahiptir ve kanser tedavisinde kullanılmak üzere beyaz ışık yoluyla kolayca eksprese edilebilir. Tasarladığımız AIEjenlerin ROS üretebildiğini doğrulamak için, singlet oksijen algılamada ticari bir sensör olan 9,10-antrasenediyl-bis(metilen)-dimalonik asit (ABDA) kullandıldı ve her iki AIEjenin de beyaz ışık ışınlaması altında ROS üretme yeteneğine sahip olduğu gösterildi. Hücre içi ROS üretimi DCFH-DA kullanılarak konfokal mikroskopi yoluyla araştırılmış ve üretilen moleküllerin beyaz ışık ışınlaması altında hücre içi ROS üretebildiği raporlandı. Her iki molekül de memeli hücreleri için güçlü bir afiniteye sahiptir ve plazma membranını kolayca boyayabilir. Yüksek ROS üretimi ve memeli hücrelerine karşı güçlü afiniteden esinlenerek, her iki AIEjenin de beyaz ışık ışınlaması altında MCF-*7* meme kanseri hücrelerini öldürebildiği gösterildi. Nano agregatların boyutları dinamik ışık saçılımı ve taramalı elektron mikroskobu ile incelendi. Kanser hücrelerine karşı etkili kullanımından esinlenerek, tasarlanan moleküllerin kanserin fotodinamik tedavisinde potansiyel olarak pratik uygulamalar bulacağı öngörülmüştür.

Anahtar Kelimeler: Floresan Moleküller, Agregasyon İndüklenmiş Emisyon, Fotosensitizerler, Hücre Görüntüleme, Fotodinamik Terapi

CONTENTS

DESIGN AND SYNTHESIS OF COUMARIN-BASED FLUORESCENT MOLECULES FOR PHOTODYNAMIC THERAPY OF CANCEROUS CELLS

CHAPTER 4

CONCLUSION AND SUGGESTIONS

ABBREVIATIONS

ABDA	: 9,10-Anthracenediyl-bis(methylene)di malonic acid
AIE	: Aggregation induce emission
CLSM	: Confocal llaser scanning microscopy
DCFH-DA	: Dichlorofluorescein diacetate
DID	: 1,1-Dioctadecyl-3,3,3,3-tetramethylindodicarbocyanine
ER	: Endoplasmic reticulum
GPX	: Glutathione Peroxidases
HpD	: Hematoporphyrin derivative
Ld	: Lipid
LPO	: Lipid peroxidation
MB	: Methylene blue
PDT	: Photodynamic therapy
PSs	: Photosensitizers
RT	: Room temperature
SEM	: Scanning electron microscopy
STEM	: Scanning transmission electron microscopy
UCNPs	: Up-conversion nanoparticles
VEGF	: Vascular endothelial growth factor

LIST OF FIGURES

LIST OF SCHEMES

CHAPTER 1

GENERAL INFORMATION AND LITERATURE REVIEW

1.1. History of Photodynamic Therapy

Throughout history, light has been a valuable tool for treating illnesses. Ancient societies like Egypt, India, and China used light therapy to address skin conditions. Photochemotherapy, which dates back centuries, involved the use of substances like psoralens [1,2]. These were employed in India around 1400 BC, according to the Atharva Veda, for regimentation treatments. In Egypt, sunlight was culturally significant and used in heliotherapy. The Ebers papyrus, an ancient medical text, mentioned vitiligo treatment around 1500 BC (Figure 1.1). Egyptians utilized psoralen extracted from the Ammi majus plant for treating leukoderma in the 12^{th} century AD. Herodotus records that heliotherapy was developed in ancient Greece to treat a variety of ailments. In later centuries, sunlight therapy was applied to conditions like tuberculosis and rickets. Modern light therapy began in the 20^{th} century, notably with Niels Ryberg Finsen's research, which earned him the 1903 Nobel Prize in Physiology or Medicine [3]. The inception of PDT in medicine dates back over a century, originating from observations of microorganism inactivation. This led to the formulation of the concept of photodynamic action, with Hermann von Tappeiner introducing the term "photodynamic reaction" to emphasize light's pivotal role. Photodynamic therapy, which leverages reactive oxygen species (ROS) to disrupt and eliminate microbes, demonstrated efficacy against both bacteria and viruses. However, due to disruptions caused by the World Wars, further development of PDT was delayed for nearly six decades [4].

Figure 1.1. Ancient method for treatment by using light [5]

Research at the Mayo Clinic by R. L. Lipson and S. Schwartz in 1960 opened a new chapter in PDT when Schwartz created hematoporphyrin derivative (HpD) to maximize tumor localization. Lipson's research demonstrated the potential of an acetic acid sulfuric acid derivative of hematoporphyrin for the detection of malignant diseases [6,7]. This HpD mixture, which included a variety of porphyrins, was first used to detect tumors and, subsequently, to treat bladder cancer. Dougherty's transformation of HpD into a drug formulation was the result of further advancements, and in 1978, the first clinical case of PDT was reported in a patient who had metastatic breast cancer to the skin (Figure 1.2). Photofrin (porfimer sodium) phase II clinical trials for early-stage lung cancer were carried out, which helped to open the door for PDT's regulatory approvals for several cancer types [8, [9].

Figure 1.2. Using light for medical treatment in the modern era [10]

For over a century, PSs (PSs) have been used as therapeutic agents. In Figure 1.3, the PDT timeline is displayed. One of the earliest PDT uses might be the clinical application of eosin in the management of skin cancer. Topical eosin was the method Tappeiner and Jelinek intended to use to treat skin tumors [11-13].

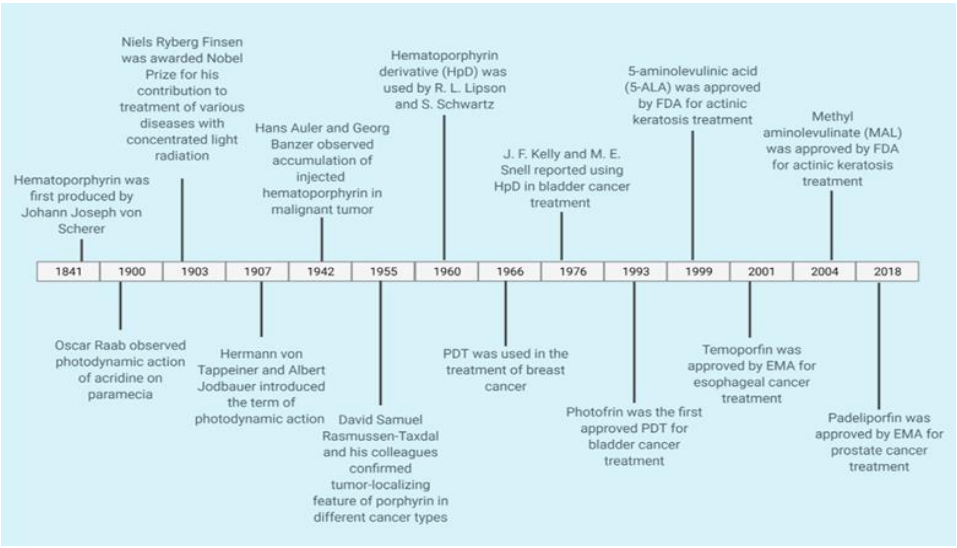

Figure 1.3. The timeline represents the application of PDT for cancer treatment [1]

PDT offers several benefits over traditional methods such as radiation, chemotherapy, and surgery. The noninvasive nature of this approach, along with its minimal side effects, lack of drug resistance, and ease of combination with other therapies, make it an appealing

option [14]. The characteristics of the PSs utilized have a major impact on PDT's efficacy. However, a common drawback of current PSs is their inability to deeply penetrate tissues due to light absorption in the UV-visible range. Researchers are concentrating on creating PSs that react to near-infrared (NIR) light to address this. NIR light is less damaging to normal cells and can penetrate tissues deeper [10].

In this field, the exciting development is two-photon excitation (TPE) PDT. In comparison to conventional techniques, it offers greater precision and allows for deeper penetration into tumors using NIR-pulsed lasers to excite PSs. Furthermore, by absorbing several photons and releasing high-energy fluorescence, up conversion nanoparticles (UCNPs) exhibit promises in PDT and enable successful treatment of deeply ingrained tumors [15,16].

Even with these developments, creating PSs with ideal characteristics like retention duration, biocompatibility, and ROS generation efficiency is still difficult. To increase the effectiveness of PDT, researchers are investigating a variety of PS classes and techniques, such as enhancing photoinduced electron transfer and energy transfer processes [17-18].

1.2. Photodynamic Therapy

Light, substrate, and a photosensitizer are the three main ingredients of PDT. PS molecules undergo an excited singlet state (S1) upon being exposed to light, which is followed by intersystem crossing (ISC) to reach the first excited triplet state (T1). When PS molecules interact with a substrate, usually oxygen, at this T1 state, ROS is produced, which interact with cellular protein and lipids and result into cell death, as shown in Figure 1.4. Based on the underlying photophysical and photochemical mechanisms, PDT can be divided into two types [19, 20].

1.2.1. Type I PDT

In type I PDT short-lived free radicals are created, when PS molecules and substrates exchange electrons from one another, these radicals react quickly with oxygen and water molecules, producing hydroxyl radicals (·OH), superoxide anion (O^{-2}), and hydrogen

peroxide (H_2O_2). PSs that are appropriate for type I processes usually have low oxidation potential and strong electron-donating capabilities [19-21].

1.2.2. Type 2 PDT

In type II PDT, triplet oxygen ($^3O_2$) is created through the energy transfer from PS molecules in their t1 state, which produces cytotoxic singlet oxygen ($^1O_2$). In PDT, type I and type II processes frequently take place concurrently. The relative sizes of these processes are determined by various factors, including PS concentration, substrate and PS properties, and environmental circumstances [11].

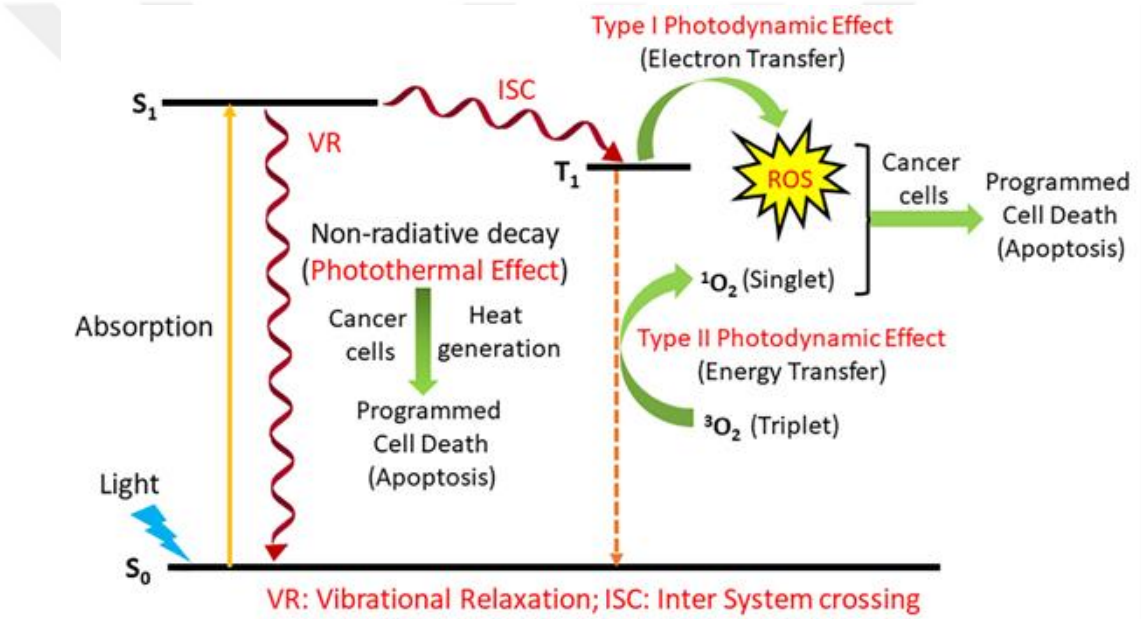

Figure 1.4. Simplified Jablonski diagram for photothermal and photodynamic effects [22]

1.3. Reactive Properties of ROS

Reactive oxygen species generally include a variety of molecules, including O_2, O^{2-}, OH^-, H_2O_2, and $^1O_2$. Ozone (O_3), hypochlorous acid (HOCl), hypobromous acid (HOBr), hypoiodous acid (HOI), peroxyl radicals (ROO), alkoxyl radicals (RO), semiquinone radicals (·SQ), carbonate radicals (·CO_3), and organic hydroperoxides (ROOH) are also included in a more comprehensive definition. ROS has two functions in living things [23-25]. They maintain homeostasis and proliferation in healthy cells at the right concentrations, and they can even alter protein structures to shield cells from outside threats. Cells use an antioxidant system made up of nonenzymatic substances like

glutathione and vitamin C, as well as enzymes like superoxide dismutase, to keep ROS levels within a reasonable range. On the other hand, oxidative damage happens when the equilibrium between the production of ROS and detoxification fails, and this is the fundamental cause of PDT-induced cytotoxicity. Through several processes, such as apoptosis, necrosis, vascular impairment, and immune responses mediated by inflammation, PDT encourages oxidative damage in tumor tissues [6, 25-29].

The degree of reactivity and selectivity that ROS displays toward distinct molecules varies. One example of a reactive electrophile is $^1O_2$, which reacts preferentially with electron-rich receptors such as aromatic hydrocarbons, indoles, and carbon-carbon double bonds. On the other hand, OH^- is a strong oxidant that interacts with almost all biological molecules, such as proteins, lipids, DNA, and RNA, as well as antioxidants [3, 27-29].

1.4. Aggregation Induced Emission

Usually, the planner structures of traditional PSs cause problems because of π–π stacking, such as reduced fluorescence signals and decreased efficacy at higher concentrations. Furthermore, imaging precision is hampered by their continuous emission of fluorescence [13].

1.5. AIE Based Photosensitizers

In contrast to conventional PSs, AIE PSs are more useful in PDT because they produce more ROS when aggregated. AIE has become a viable option for PDT and fluorescence imaging. Because of their special optical properties, they can be used to create light-up probes that will increase photosensitization efficiency and imaging sensitivity [30]. The efficacy of AIE PSs were increased by improved intersystem crossing (ISC). As an alternative, a more useful strategy is to encourage ISC by lowering the energy gap between singlet and triplet states (DEST). To lessen valence electron repulsion, the highest occupied molecular orbital (HOMO) and lowest unoccupied molecular orbital (LUMO) are separated via the donor–acceptor (D–A) molecular engineering techniques, demonstrated the efficacy of this approach by creating AIEgens with varying degrees of HOMO–LUMO separation based on the tetraphenyl ethylene (TPE) framework [25].

1.6. Introduction to Photosensitizers

In PDT, PSs are as important as light and oxygen. Their capacity to absorb light at certain wavelengths and cause photochemical or photophysical reactions. Ideal PSs have a specific set of properties and requirements, which are listed below,

1. High chemical purity and stability at room temperature [22].
2. Photosensitivity is restricted to specific wavelengths [33].
3. High photochemical reactivity, with peak light absorption ideally between 600 nm and 800 nm. Absorption beyond 800 nm lacks the energy required to activate oxygen into its singlet state and produce other reactive oxygen species [33].
4. Absorption minimum between 400 nm and 600 nm, preventing excessive photosensitivity due to sunlight exposure [34].
5. Absorption bands that do not overlap with those of other substances in the body, such as melatonin, hemoglobin, or oxyhemoglobin [33].
6. Minimal cytotoxicity in the absence of light [35].
7. Easy solubility in bodily tissues [36].
8. High selectivity for neoplastic tissues, with slow elimination from affected areas to ensure prolonged exposure, coupled with quick elimination from healthy tissues to minimize phototoxic side effects [37].
9. Cost-effective and straightforward synthesis, ensuring accessibility [38].

1.7. Generations of Photosensitizers

PDT was first applied in medicine by first-generation PSs, which were primarily derived from naturally occurring porphyrins. Hematoporphyrin and photofrin are two examples of how PDT is used in cancer treatment. First-generation PSs had drawbacks like poor absorption and dark cytotoxicity, even though they were initially effective [39].

Second-generation PSs, such as 5-aminolevulinic acid and benzoporphyrin, were created as a result of further research and development. These substances were created to address these issues by exhibiting decreased phototoxicity and enhanced solubility. They still presented problems with tissue damage and stability, though [40].

Third-generation PSs, which involve altering current medications to improve their specificity and efficacy, are an advancement in PDT techniques as shown in Figure 1.5. To improve localization at target sites, conjugation with targeting agents or encapsulation into carriers like nanoparticles are employed. Although these developments are promising for improving PDT results, the best PSs should have characteristics like stability, low dark toxicity and high quantum yield. More clinical research is needed to assess the relative safety and efficacy profiles of various PSs, which will help shape the creation of more powerful therapeutics for PDT applications [41].

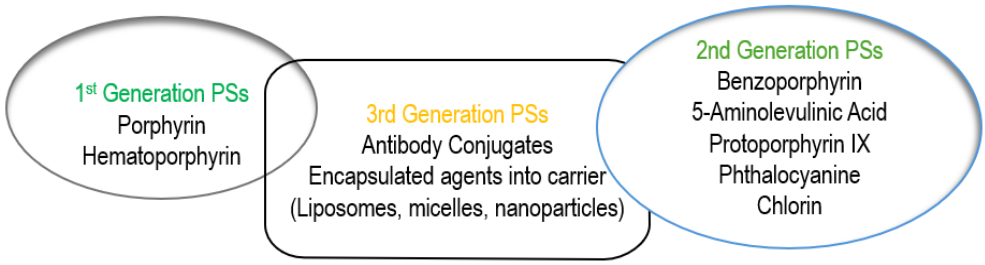

Figure 1.5. Selected examples of the 1st, 2nd, and 3rd generation of PSs

1.8. Light Source of PSs

There are two important phases in the photodynamic treatment process. The treatment is started when light expose to the PSs molecule. Light sources like argon, argon-pumped dye, metal vapor-pumped dye, solid state, optical parametric oscillators, and diode lasers are among the available laser options as shown in Figure 1.6. As an alternative, non-laser sources include fluorescent lamps, metal halide lamps, xenon arc lamps, tungsten filament quartz halogen lamps, and phosphor-coated sodium lamps. Additionally, femtosecond solid state lasers and light-emitting diodes (LED) can be employed for this purpose [42].

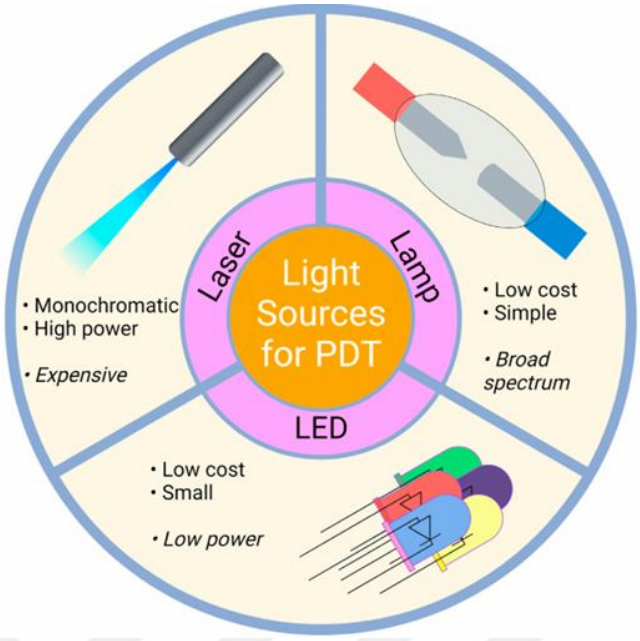

Figure 1.6. Light source utilized in PDT, lamp, laser, and LED [1]

1.9. Ideal Photosensitizers

The list of properties for an ideal photosensitizer is given below [43].

1. Nontoxic Nature: To prevent the need for substitutes to chemotherapy, the photosensitizer must be non-toxic, and its breakdown should not produce hazardous byproducts [44].
2. Anti-carcinogenicity: It should not cause cancer or mutations, making it impossible to treat one illness at the expense of another [45].
3. Elimination: To accomplish the clinically feasible removal of the photosensitizer a prerequisite for potential retreatment without re-administration its half-life must be considered [46].
4. Selectivity/targetability: If the photosensitizer is properly illuminated and activated, it should preferably accumulate in target tissues to reduce damage to healthy tissues [47].
5. Activation: Dependable activation by suitable light wavelengths is essential to prevent inadvertent treatment [46].
6. Sunlight precautions: The tendency of PSs to build up in the skin makes it imperative to take precautions against exposure to sunlight [48].
7. High Range of Administration: The photosensitizer ought to provide a range of administration options, minimal administrative hassles, and user-friendliness [49].

8. Indications: Tailored safety and efficacy are ensured by specific indications for various medical conditions [49].
9. Reliability: The photosensitizer must reliably reach target tissues and activate as needed for successful therapy [50].
10. Pain-free therapy: As outpatient therapy is common, a photosensitizer causing pain during or after treatment would hinder success [50].
11. Outpatient therapy: Patient-friendly and cost-effective outpatient administration is preferred for PDT [51].
12. Availability: Commercial availability and easy reconstitution by local pharmacies are desirable [47].
13. Cost: Wide PDT accessibility depends on cost-effectiveness [52].
14. Safety: The photosensitizer should not cause any negative side effects, such as heart attacks, strokes, or clots [53].
15. Biochemistry: While non-soluble PSs might require appropriate carriers for clinical use, water-soluble PSs can pass through the body with ease [54].
16. Wavelength: Deeper tissue penetration during activation is made possible by longer wavelengths [54, 55].
17. Integrative ability: A good photosensitizer should work in tandem with other medical interventions such as radiation, chemotherapy, and surgery [56].
18. Forgiving: To reduce the possibility of treatment overdosage, the photosensitizer should withstand excessive illumination [57].
19. Transparency: Desired characteristics in an ideal photosensitizer include clear indications of treatment success and support in reaching desired outcomes [54], [57].

1.10. Nanomaterial Based Photosensitizers

Nanomaterials based PSs, are potentially useful strategy to improve PDT efficiency. Several benefits can be obtained by adding photosensitizing agents to nanomaterial platforms, such as nanoparticles, nanocarriers, or nanocomposites [58].

Enhancing stability and solubility of photosensitizing agents is one of the main benefits of PSs based on nanomaterials. PSs can be bound or encapsulated by nanoparticles, which prevents them from breaking down and lengthens their half-life in the body. Because of its increased stability, the photosensitizer can be released at the target site under controlled conditions. PSs can be specifically delivered to diseased tissues with the help of nanomaterials. When targeting ligands like peptides or antibodies are added to

nanoparticles, they become functional and can bind and recognize specific molecular markers that are expressed on cancer cells. By minimizing off-target effects and promoting photosensitizer accumulation within tumors, this targeted approach reduces systemic toxicity and improves treatment outcomes [59].

Multimodal imaging and PDT are possible with nanomaterial-based PSs. Imaging agents, like fluorescent dyes or contrast agents, can be engineered into nanoparticles to allow real-time tumor visualization during treatment. This makes it possible to precisely track the course of treatment and evaluate the effectiveness of therapy [60]. While there are many benefits to using nanomaterial-based PSs, there are a few problems and disadvantages with PDT that need to be fixed:

Biocompatibility and Toxicity: Several nanomaterials that are utilized as photosensitizer carriers have the potential to be cytotoxic or to trigger immunological reactions in the body. It is imperative to ensure the biocompatibility of these nanocarriers to reduce any potential harm to healthy tissues [36, 61].

Nanoparticle Accumulation: Although passive or active targeting mechanisms of nanomaterials can improve the accumulation of PSs at tumor sites, there is a risk of nonspecific accumulation in organs other than tumor, which results in toxicity or off-target effects [62].

Tissue Penetration: In tissues with dense extracellular matrices or deep-seated tumors, certain nanomaterials may have limited tissue penetration depth. This may lessen the effectiveness of treatment by preventing PSs from reaching their intended locations [63].

Biodegradation and Clearance: To avoid long-term accumulation in the body, which could be harmful or interfere with regular physiological functions, the biodegradation and clearance kinetics of nanomaterials must be carefully regulated [64].

Complex Synthesis and Characterization: The synthesis of nanomaterials frequently calls for complex processes and exact control over the size, shape, and surface characteristics of the particles. Ensuring batch-to-batch consistency and characterizing these nanoparticles can be difficult and time-consuming tasks [65].

Regulatory Obstacles: Safety, efficiency, and manufacturing standards regulations present difficulties for treatments based on nanomaterials. Complying with strict guidelines and conducting extensive preclinical testing are often necessary to meet regulatory requirements for clinical translation [43].

Cost: The expense of producing and purifying nanomaterials for clinical use may prevent them from being widely used and accessed, especially in healthcare settings with limited resources [66].

1.11. Organic Photosensitizer

In contrast to nanotechnology-based PSs, organic based PSs have unique advantages, when used as PDT. The advantages of organic based PSs are as under:

Biocompatibility: Compared to heavy metal-based nanomaterials, organic PSs are less likely to cause cytotoxic effects or immune responses because they are frequently derived from natural or biocompatible materials [17].

Chemical Diversity: A wide range of chemical structures and functional groups can be synthesized into organic molecules, which makes it possible to precisely tune their photophysical and photochemical characteristics to maximize the effectiveness of PDT [54].

Targeting Efficiency: Targeting ligands or biomolecules can be readily added to organic PSs to increase their accumulation in particular diseased tissues. This improves treatment specificity and decreases off-target effects [55].

Biodistribution and Clearance: Because organic PSs can be naturally metabolized and excreted from the body, there are typically fewer long-term toxicity issues associated with them. This results in favorable biodistribution and clearance profiles [56].

Cost-Effectiveness: Compared to the production of complex nanomaterials, organic synthesis methods are frequently more scalable and cost-effective, which makes organic PSs more accessible for clinical translation and widespread adoption [17], [66].

Regulatory Approval: Compared to innovative nanotechnology-based formulations, many organic PSs have already undergone substantial preclinical and clinical evaluation for PDT applications, which may speed up their regulatory approval and clinical use.

1.12. Introduction to Coumarin

The coumarin compound, which has a vanilla-like flavor, was first extracted from tonka beans, bison grass, woodruff, mullein, lavender, licorice, strawberries, apricots, cherries, cinnamon, and sweet clover, has varied biological activity and chemical properties. Both free and combined forms of coumarin (coumarin glycoside) with glucose are possible as shown in Figure 1.7. Since 1882, it has been a common ingredient in perfumes due to its pleasant aroma, which is easily identified as that of freshly cut hay. For centuries, traditional medicine has utilized coumarins, which are naturally occurring polyphenolics that are found in a wide range of plants, fungi, and bacteria. Numerous qualities, including antibacterial, antifungal, antioxidant, anti-inflammatory, anti-HIV, anticancer, antituberculosis, anticoagulant, antiviral, and antidiabetic effects, are displayed by these compounds. Plants produce coumarin through the processes of hydroxylation, glycolysis, and cyclization of cinnamic acid. Due to its ability to suppress appetite, coumarin may be found in many plants, particularly grasses, where it lessens the negative effects of grazing [8]. Coumarins hold a significant place in both natural and synthetic organic chemistry because of their possible uses in the fragrance, pharmaceutical, and agrochemical industries. Certain derivatives can inhibit acetylcholinesterase, which could be useful in the treatment of cancer. It also emphasizes the broad applications of coumarins in drug development [9].

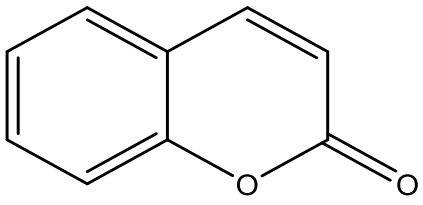

Figure 1.7. Coumarin Core

Because so many natural products have this heterocyclic nucleus, organic and medicinal chemists have long been interested in the synthesis of coumarins and their derivatives. Coumarins are extensively used as additives in food, fragrances, cosmetics,

pharmaceuticals, dispersed fluorescent and laser dyes, insecticides, and optical brighteners [3]. Many of the widely distributed, physiologically active substances found in plants, known as coumarins, have been used in traditional medicine for thousands of years. Coumarins have a variety of pharmacological properties, including antibacterial, anti-HIV, anticancer, and anticoagulant properties. Among coumarins' many properties, their antibacterial and anticancer properties stand out. Numerous structurally unique coumarin derivatives have demonstrated strong cytotoxic effects both in vivo and in vitro. Furthermore, their inhibitory effect on inflammatory cells outperformed that of any other clinically available substance. The medicinal potential of specific coumarins is obvious, since it is known that certain substituents are necessary to increase their actions [9, 67]. Numerous methods have been developed for the synthesis of coumarins due to their natural occurrence, useful range of biological activity, and diverse pharmacological properties. Pechmann, Perkin, Knoevenagel and Wittig reactions are among the traditional pathways to coumarin. Many coumarin derivatives have been identified from natural sources; the patterns of substitutions determine the pharmacological and biochemical characteristics of these compounds [5, 9].

1.13. Synthesis

1.13.1. Knoevenagel Reaction

Knoevenagel reaction follow the principle of aldol condensation that forms carbon-carbon bonds, when an aldehyde or ketone with an active hydrogen compound is present in organic solvents along with a basic catalyst like piperidine, pyridine, ammonia, or sodium ethoxide [67] as shown in scheme 1.1.

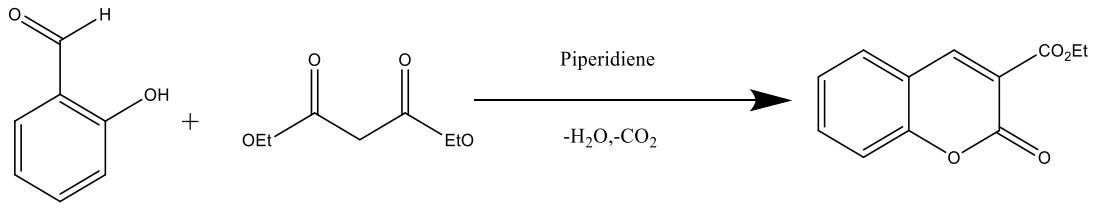

Scheme 1.1. Preparation of Coumarin by the Knoevenagel method.

1.13.2. Perkin Reaction

Perkin originally presented the condensation reaction of simple salicylaldehyde in the presence of acetic anhydride as a means of constructing coumarin in 1968. A basic reaction condition was met for the Perkin reaction of salicylaldehyde and acetic anhydride, which resulted in α, β-unsaturated aromatic acid in the presence of sodium acetate and intramolecular cyclization that produced the expected substituted coumarin [9] as shown in scheme 1.2.

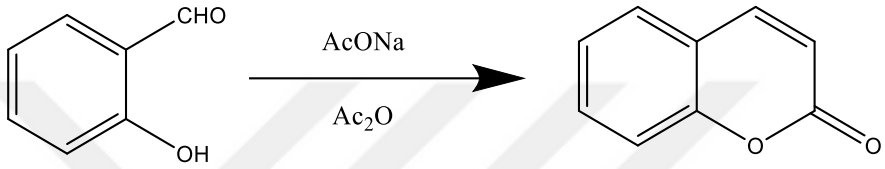

Scheme 1.2. Preparation of coumarin by the Perkin method.

1.13.3. Wittig Reaction

German chemist Georg Wittig made the discovery of this reaction known by its Wittig name. In 1979, he was awarded the Nobel Prize in Chemistry for discovering this important olefin synthesis. When aldehyde or ketone is combined with a triphenyl phosphonium ylide, a Wittig phosphine reagent, the reaction produces phosphine oxide as a byproduct and the anticipated olefin in good yields. Both drug molecules and extremely significant natural products can be prepared using this system. Kumar et al. followed the Wittig reaction route to prepare a variety of substituted coumarin derivatives from corresponding phenols with an ortho-carbonyl group and triphenyl (α carboxymethyl ene) phosphorane imidazole ylide. A good yield of olefin was reported. The reaction's mechanism implies that the phosphorane intermediates are involved in the process. The literature contains several reports on the synthesis of coumarin scaffolds using the Wittig reaction, which begins with an aldehyde or ketone and ends with phosphonium ylide [48] as shown in scheme 1.3.

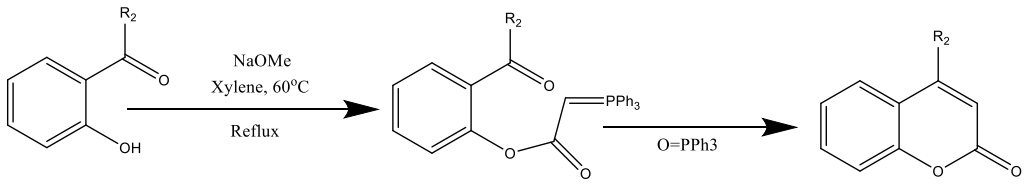

Scheme 1.3. Preparation of Coumarin by Witting reaction.

1.14. Targeted Based Photodynamic Therapy

PDT is recognized as an appealing therapeutic method due to its ability to selectively eliminate targeted cells or tissues with minimal adverse effects. However, the difficulty of selectively delivering PSs has hindered the clinical application of PDT. Recent research has focused on developing strategies to enhance both the selectivity of PSs and the overall efficacy of PDT [70]. One such approach involves conjugating PSs to antibodies, enabling site-specific delivery without altering their biochemical properties. These PSs - antibody conjugates, known as immunoconjugates, accumulate in targeted tumor cells, thereby reducing the risk of damage to healthy tissues. Studies have shown that immunoconjugates exhibit high selectivity for tumor cells and demonstrate enhanced phototoxic effects in response to PDT [71]. For instance, immunoconjugates of the PSs pyropheophorbide-a with anti-HER2 monoclonal antibodies significantly improved the efficacy of PDT in breast and ovarian cancer cell lines. However, despite promising results, antibody-targeted PDT has not yet been widely adopted for clinical use due to challenges such as the detection of ideal antigens and potential hindrance by large antibody molecules [72].

To overcome these limitations, researchers have explored alternative targeting strategies, such as conjugating PSs to small molecules or peptides. For example, folate receptor-targeted PDT utilizes PSs conjugates recognized by folate receptors overexpressed in cancer cells, leading to selective delivery to cancer cells in vitro and in vivo. Similarly, conjugating PSs to oligoarginine peptides or aptamers has shown promise in targeting tumors effectively [73]. The key principle of PDT is the use of PSs that, when exposed to specific wavelengths of light, produce cytotoxic reactive oxygen species, leading to cancer cell death as shown in Figure 1.8.

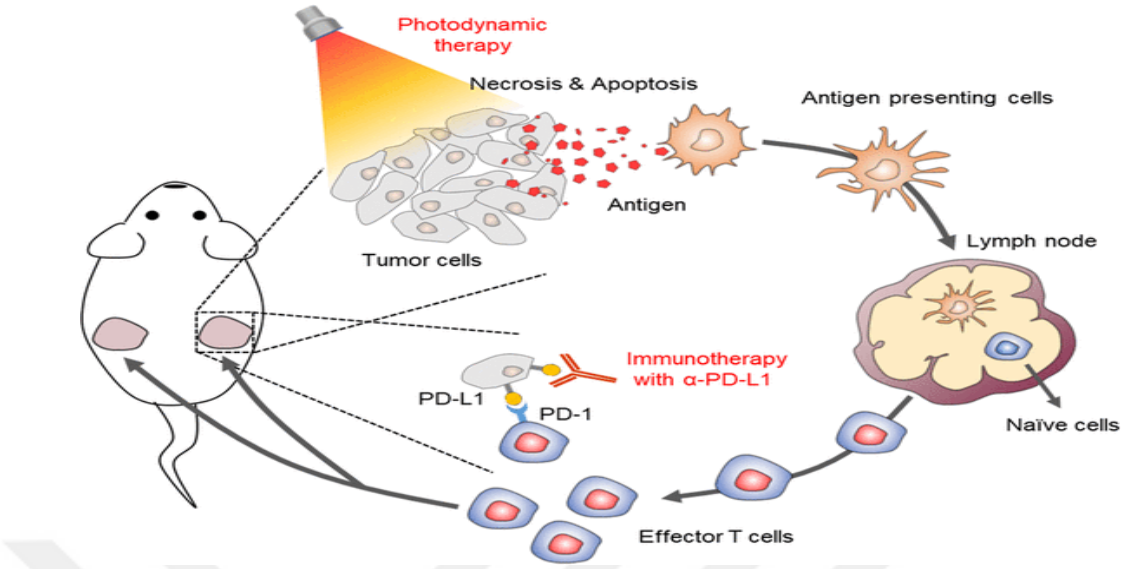

Figure 1.8. Killing of cancerous tumor cells by PDT [24]

However, the effectiveness of PDT largely depends on the choice of PSs. Many of the currently available PSs have limitations, including low singlet oxygen quantum yields, inadequate cancer cell targeting, and poor photostability. These limitations necessitate the development of more effective and selective PSs to enhance the efficacy and safety of PDT in cancer treatment [74].

Apoptosis is distinguished by hallmark cellular changes, including cellular shrinkage, chromatin condensation and fragmentation, cell blebbing, and the formation of apoptotic bodies. Notably, during apoptosis, there is no leakage of cellular contents. Necrosis is characterized by cytosol and organelle swelling, followed by membrane breakdown and the release of cellular contents into the surrounding environment [76]. Autophagy involves the formation of autophagosomes, which encapsulate cellular components targeted for degradation, followed by fusion with lysosomes to form autolysosomes as shown in Figure 1.9. While autophagosomes and autolysosomes are the primary features of autophagy, vacuolization may also occur in some instances [77]. These advancements in PDT protocols demonstrate significant progress in more effective cancer treatments, offering hope for improved outcomes and reduced side effects for patients.

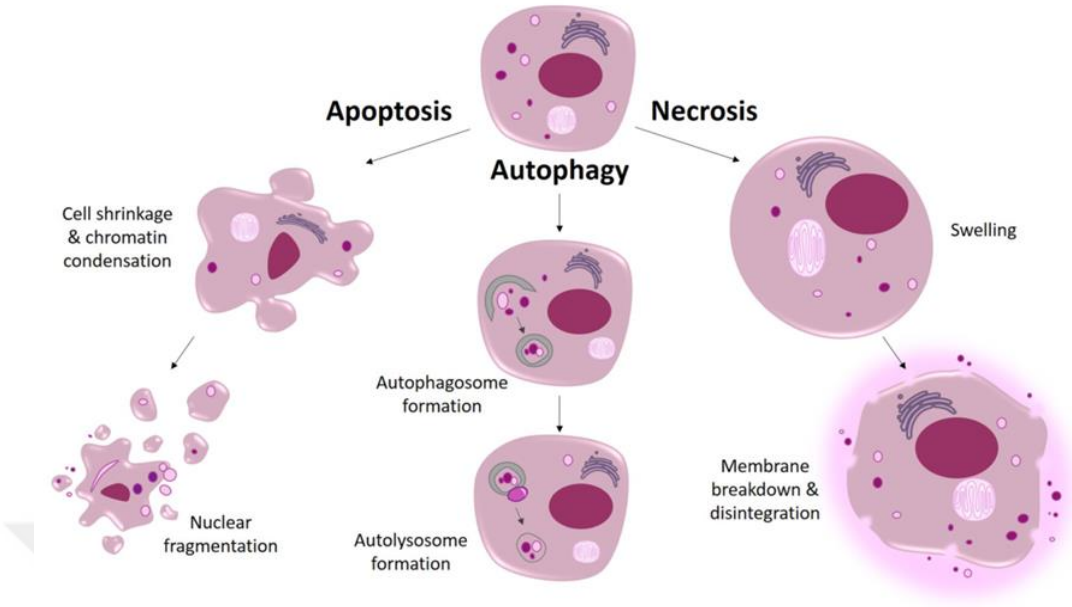

Figure 1.9. The three most noted pathways of cell death [75]

1.15. Organelle Targeting Photosensitizers

Subcellular organelles play crucial roles in cellular function, and their disruption can lead to cell dysfunction and death. Therefore, achieving precise targeting of PSs to specific organelles holds significant potential for improving the efficacy and safety of PDT. By targeting PSs to organelles, it becomes possible to reduce PS dosage, minimize side effects, avoid drug resistance, and enhance therapeutic outcomes. Organelle-targeted PSs represent a novel approach for developing the next generation of PSs and offer promising strategies for advancing precision medicine [78].

The recent targeting strategies aimed at different organelles, along with the corresponding design principles for molecular and nanostructured PSs. These strategies encompass a variety of approaches, including ligand conjugation, subcellular localization signals, and nanocarrier-mediated delivery, among others as shown in Figure 1.10. By leveraging these targeting strategies, researchers can precisely direct PSs to specific organelles such as mitochondria, lysosomes, endoplasmic reticulum, and nuclei, thereby enhancing PDT efficacy while minimizing off-target effects [79].

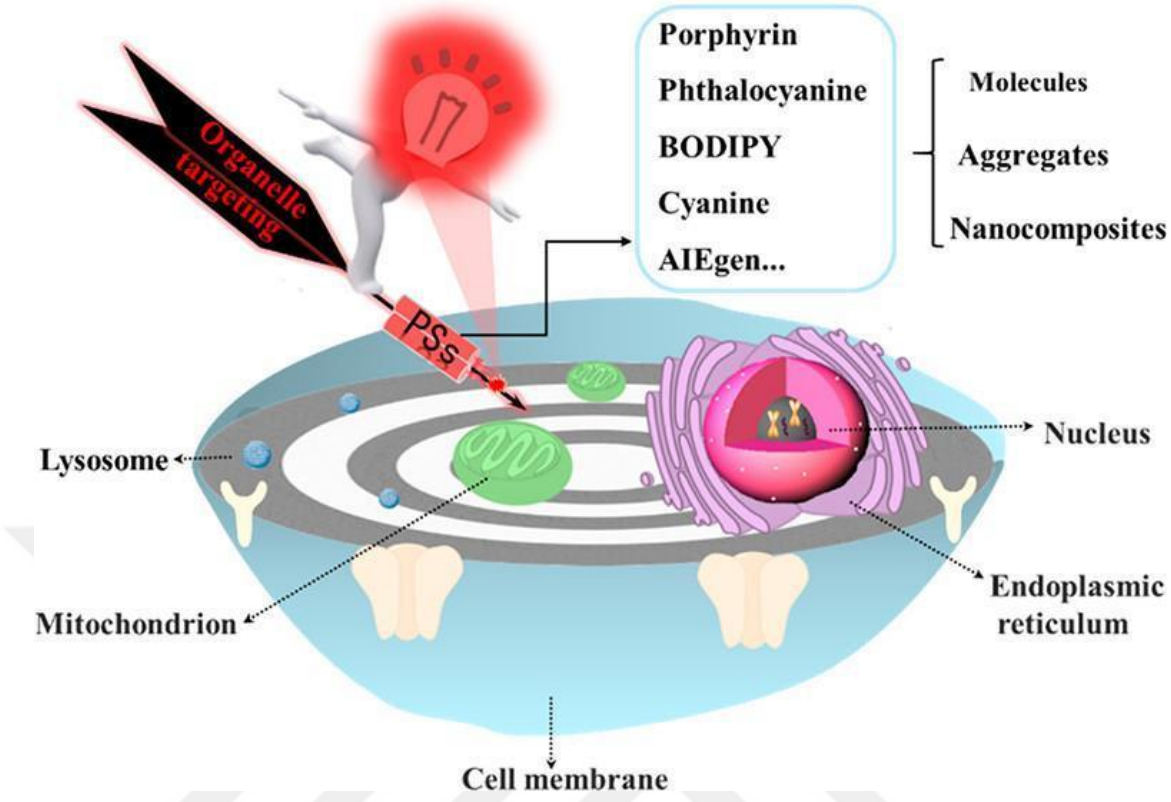

Figure 1.10. An innovative approach to PDT by specific designed PSs with different organelle-targeting abilities [80]

1.15.1. Endoplasmic Reticulum Targeting Photosensitizers

Two novel Type I PSs with effective type I ROS generation capabilities, α-TPA-PIO and β-TPA-PIO, were previously reported. They are derived from isomers of phosphindole oxide. To provide insight into the molecular architecture of PSs based on the type I mechanism, a thorough investigation of photophysical and photochemical mechanisms was carried out. The in vitro findings show that these two PSs can effectively trigger ER-stress-mediated apoptosis and autophagy in PDT by selectively accumulating in a neutral lipid region of cells, specifically in the endoplasmic reticulum (ER) [80-86]. According to in vivo models, α -TPA-PIO is capable of remarkable tumor ablation. The ER stress based on ROS that is induced by PDT mediated by β-TPA-PIO has great potential to serve as a precursor to the immunostimulatory effect in immunotherapy as shown in Figure 1.11. A thorough protocol for type I-based, purely organic PSs is presented in this work [23].

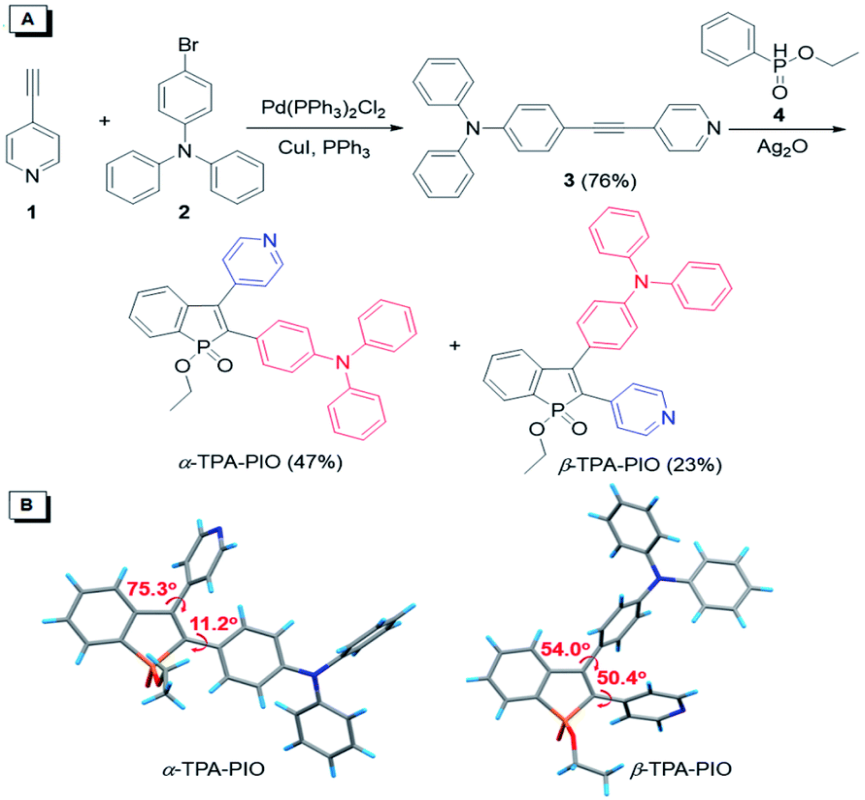

Figure 1.11. (A)The synthesis route and mechanism of α-TPA-PIO and β-TPA-PIO PSs (B) Torsion angles and packing mode of α-TPA-PIO and β-TPA-PIO [23]

1.15.2. Nucleus Targeting Photosensitizers

A major challenge still lies in designing biologically active PSs that combine PDT and chemotherapy in an efficient manner. Reported CQA which was a biologically active photosensitizer that targets DNA by combining the photosensitizing moiety with the DNA alkylating moiety chlormethine. CQA has been shown to function as an efficient DNA-targeting and damage-causing chemotherapeutic agent via chlormethine through DNA damage experiments and molecular docking. Meanwhile, when exposed to light, CQA can significantly increase DNA damage [82], [83]. The addition of the anthraquinone group, which has favorable redox characteristics and functions as an electron acceptor to encourage electron transfer, is thought to be responsible for this improvement presented in Figure 1.12. As a result, CQA effectively produces ROS of both type I and type II, which has a positive effect on PDT. Results from H&E staining, IHC analysis, and in vivo tumor growth experiments have validated the antitumor efficacy of CQA. The design of the study draws attention to targeted DNA damage and

increased ROS production. This shows how important it is to use chemo and PDT together to create effective cancer treatments [83].

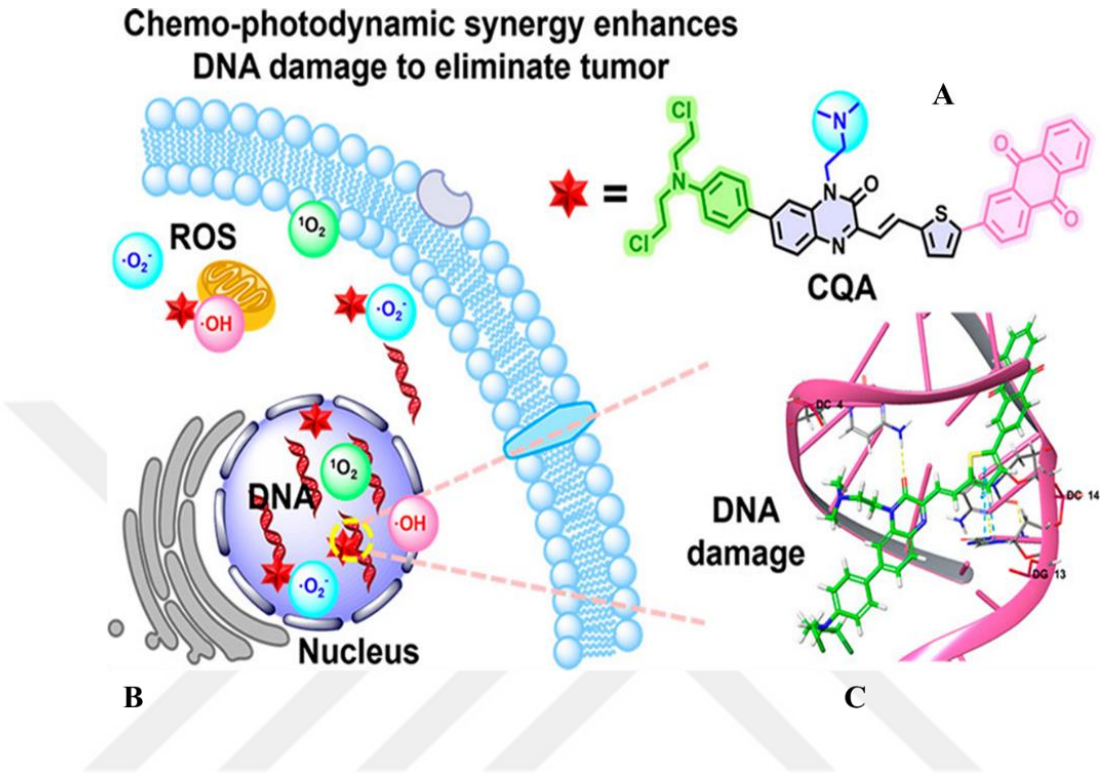

Figure 1.12. (A) Structure of CQA PSs (B) Intracellular ROS generation in the nucleus (C) DNA damage because of oxidative stress [83]

1.15.3. Lysosome Targeting Photosensitizers

The reported pyridine-embedded phenothiazinium dye acted as highly effective and potent PSs to selectively localize to lysosomes and photosensitivity to kill cancer cells. These dyes could be easily synthesized in a few short steps. Compound 5 was one of the most effective in killing large solid tumors (approximately 300 mm^3) in a xenograft mouse model without causing any apparent side effects. It was able to promote intracellular ROS upon light irradiation by nearly 40-fold higher than that of methylene blue (MB), a general phenothiazinium-based PS, presented in Figure 1.16. Compound 5 also demonstrated an impressive phototherapeutic index (PI = 53.8) against HT29 cancer cells. According to these findings, compound 5 of the pyrido-phenothiazinium dyes developed here may be a promising lysosome-targeted PS for effective photodynamic antitumor therapy [8] as shown in Figure 1.13.

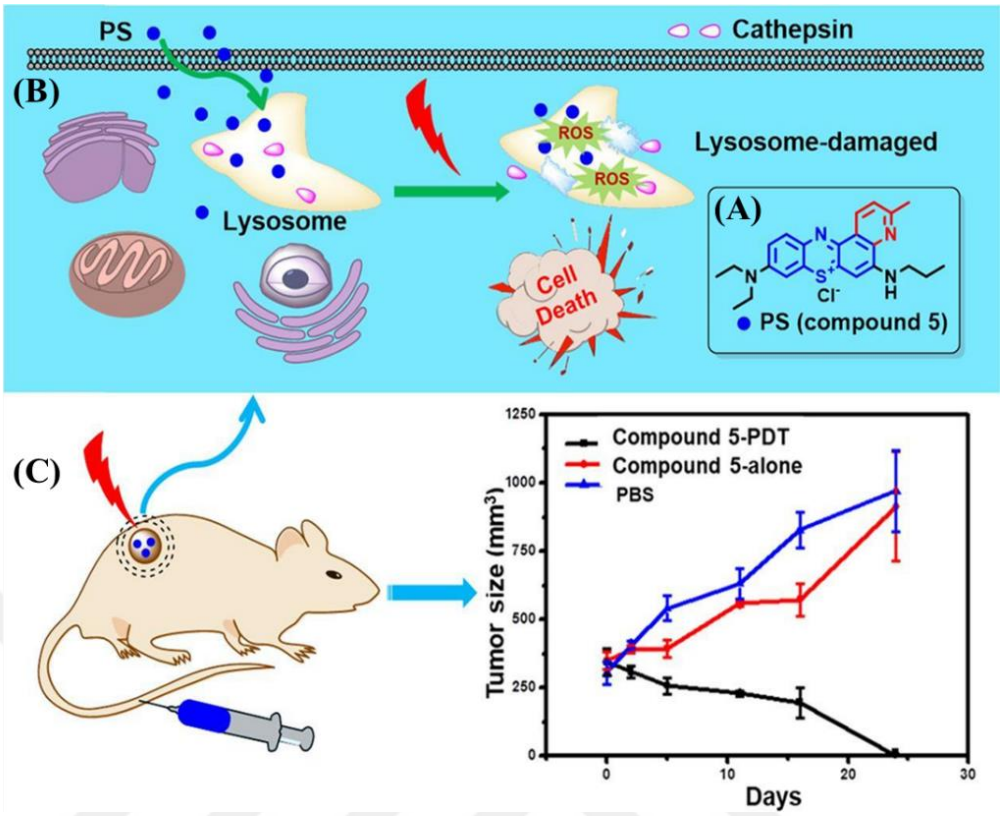

Figure 1.13. (A) Structure of PS (Compound 5) (B) Accumulation of PSs in lysosomes inside the cancerous cell (C) In vivo Analysis [8]

1.15.4. Lipid Droplet Targeting Photosensitizers

Ferroptosis holds potential as an anti-tumor treatment since it is an iron-dependent lipid peroxidation (LPO)-mediated cell death pathway [59]. The best method for producing ROS for lung pain is PDT [84]. On the other hand, the typical PDT typically targets subcellular organelles like the lysosome, mitochondria, and endoplasmic reticulum, resulting in rapid cell death prior to ferroptosis. The first type I PS targets lipid droplets (Ld) and has increased production of superoxide anion (O^{2-}), known as MNBS, is described here. After irradiation, the newly designed PS selectively localizes at Ld in cells and causes cellular LPO accumulation by producing enough O^{2-}. This leads to ferroptosis-mediated chronic PDT, which achieves highly effective anti-tumor PDT in both normoxia and hypoxia. Comprehensive characterizations and theoretical calculations suggest that the dispersed molecular electrostatic distribution-induced elevated H-aggregation tendency is the source of the MNBS's Ld targeting property and enhanced O^{2-} generation. Additional in vivo investigations employing liposomes encapsulated with MNBS showcase the remarkable anti-cancer and anti-metastatic

properties. This work presents a type I PS paradigm reinforced by H-aggregation for ferroptosis-mediated PDT [85] as shown in Figure 1.14.

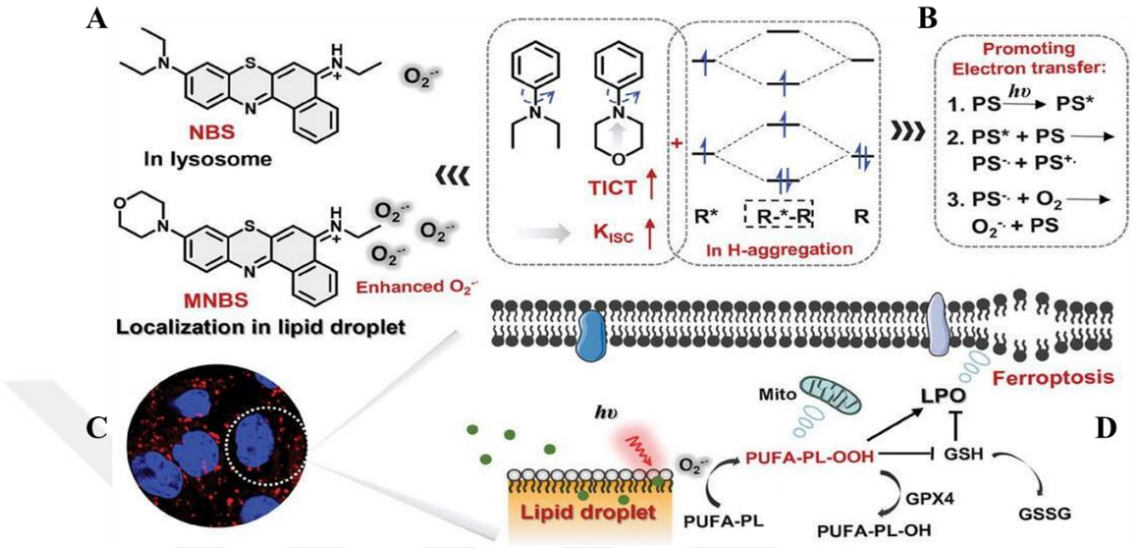

Figure 1.14. (A) Lipid droplet localized structure (MNBS) (B) with enhanced singlet oxygen generation capability (C) Confocal images of MNB staining Ld of cancerous cells (D) Intracellular ROS generation in cancerous cells [85]

1.15.5. Plasma Membrane Targeting Photosensitizers

Cell plasma membrane is the primary barrier that protects cells from the extracellular environment and facilitates diverse biological processes, including immunologic response elicitation, signal transduction, and inorganic ion trafficking [68]. Cell plasma membrane is an ideal target for PDT [32]. Na Zaho et al. recently reported TPE-based AIEgens (TPTB and TPTH) [68], which efficiently generated ROS through both energy and electron transfer pathways. The presence of bromine (Br) in TPTB enhances its ROS generation efficiency due to the heavy atom effect. Moreover, TPTB optimal lipophilicity enables it to selectively image the cell plasma membrane with high specificity and long-term retention capability. Importantly, TPTB appropriate lipophilicity also allows it to withstand changes in plasma membrane potential. By efficiently generating ROS, TPTB demonstrates a membrane-targeted PDT effect, effectively eliminating cancer cells. This research presents a valuable molecular tool for investigating the mechanisms underlying membrane-associated cellular homeostasis as shown in Figures 1.15. and 1.16 [7, 26].

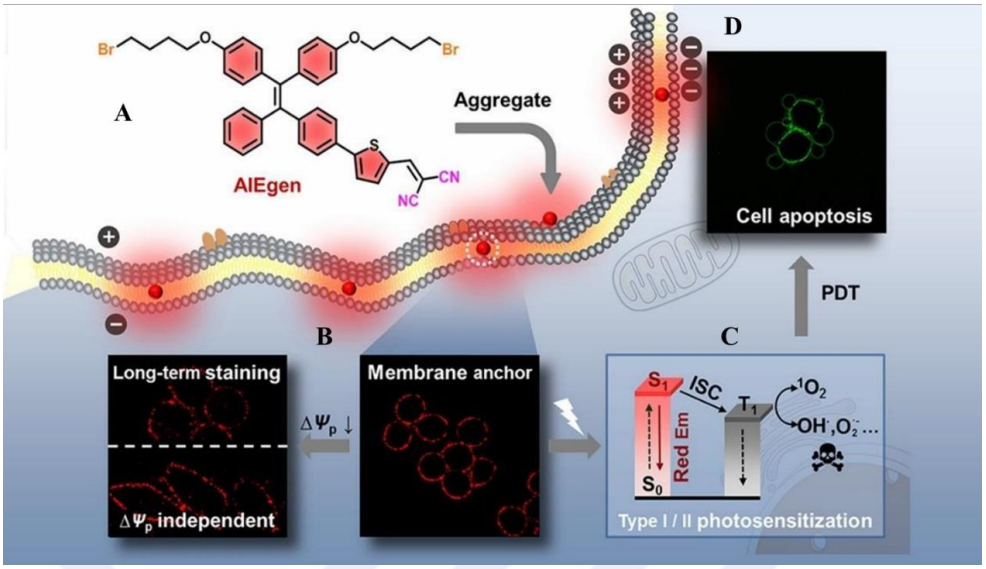

Figure 1.15. (A) Structure of TPTB (B) Confocal cell images of TPTB staining on Cell plasma membrane (C) Mechanism of ROS generation (D) Cell death images under confocal microscope [25]

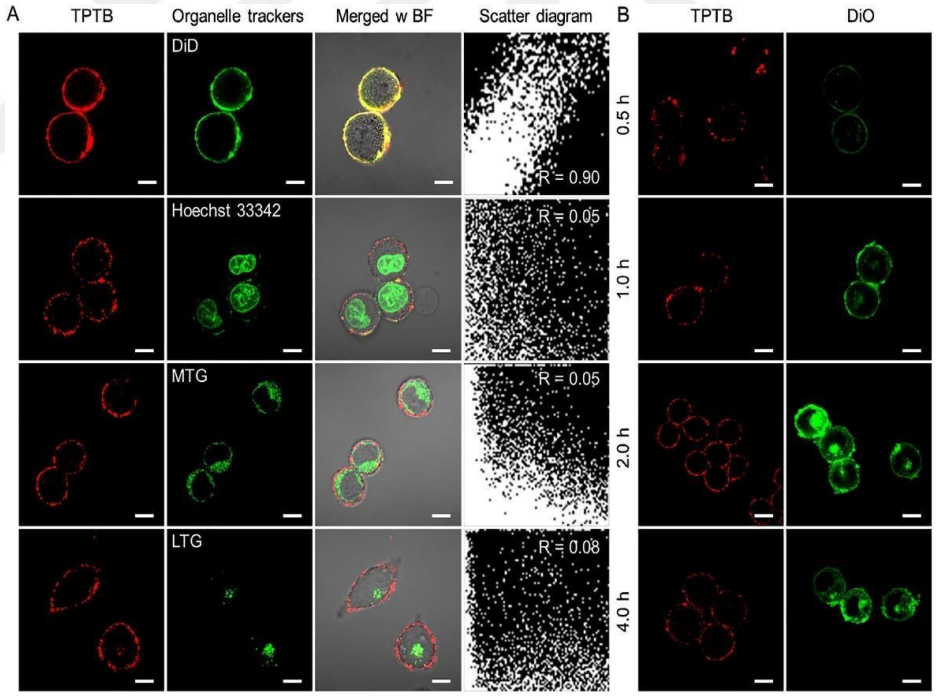

Figure 1.16. Confocal laser scanning microscopy (CLSM) images were obtained of HeLa cells co-stained with TPTB at a concentration of 10 μmol/L, along with various organelle trackers. The images reveal the spatial distribution and co-localization of TPTB with different cellular organelles. Additionally, long-term images were captured of HeLa cells treated with TPTB or DiD, providing insights into the temporal dynamics of TPTB uptake and localization within the cells. The scale bar in the images represents 10 μm, providing a reference for the size of the observed cellular structures [25].

In conclusion, coumarin was used for the synthesis of various medical drug, because of the efficient results and easily availability of coumarin in nature. coumarin based photosensitizers are not much explored for the PDT applications, thus we designed novel photosensitizers based on that coumarin core. Plasma membrane is proved to be the most suitable and effective place for the targeted PDT [25]. The designed PSs are specifically targeted towards plasma membrane and have strong binding ability with excessively present phospholipids in plasma membrane by using electrostatic and hydrophobic interaction Figure 1.17.

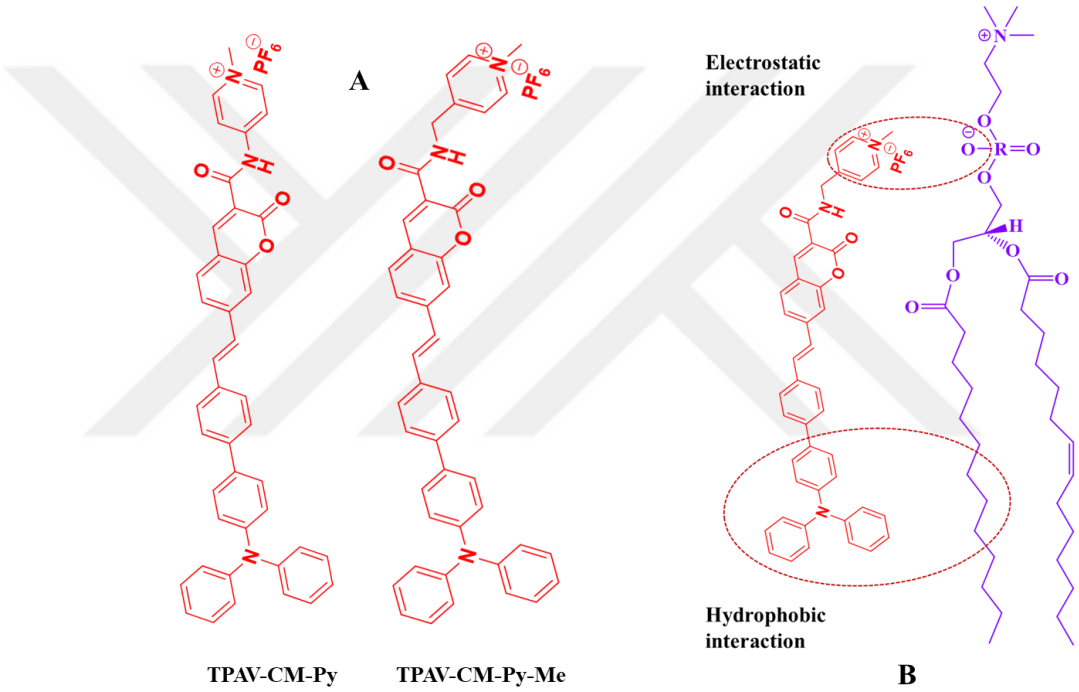

Figure 1.17. (A) Represent the molecular structures of designed TPAV-CM-Py-Me and TPAV-CM-Py photosensitizers (B) Interaction of designed photosensitizers with phospholipids of cell membrane

CHAPTER 2

MATERIAL AND METHODS

2.1. Chemicals and Reagents

Listed below, chemicals and apparatus for In vitro analysis were purchased from (Sigma Aldrich) Germany.

1. 4-Bromo-2-hydroxybenzaldehyde
2. Ethyl acetate
3. Piperidine
4. Sodium hydroxide
5. Ethyl acetoacetate
6. Ammonium acetate
7. Acetic acid
8. Toluene
9. Sodium carbonate
10. Tetrakis (triphenylphosphine)palladium
11. Acetonitrile
12. Methyl iodide
13. Acetone
14. Potassium hexafluorophosphate
15. 1-Bromo-4-vinylbenzene
16. Palladium (II) acetate
17. Tri(o-tolyl) phosphine
18. Triethylamine
19. Various laboratory solvents (e.g., dichloromethane, n-hexane, petroleum ether)

20. Cell culture media and related materials for in vitro testing

2.2. Laboratory Equipment

The chemical structures of the intermediates and final products were characterized by nuclear magnetic resonance (NMR) spectroscopy (via a Bruker DRX-400 MHz spectrometer) in DMSO-*d6* at room temperature. UV− vis spectra were recorded with a UV− vis spectrophotometer (Perkin Elmer Lambda-25). Molecular size was recorded on Zetasizer (Malvern Nano ZS-90). SEM and STEM images were recorded on an Electron Microscope (ZEISS GEMINI-500). Fluorescence spectra were recorded on a fluorescence spectrofluorophotometer (Cary Eclipse - Germany). A confocal laser scanning microscope (ZEISS LSM-900, 63x /oil confocal mode) was used to record the confocal images.

2.3. Procedure of TPAV-CM-Py-Me and TPAV-CM-Py Photosensitizer Synthesis

TPAV-CM-Py-Me and TPAV-CM-Py were synthesized through multi-step synthetic protocol. Designed PSs represent in Figure 2.1.

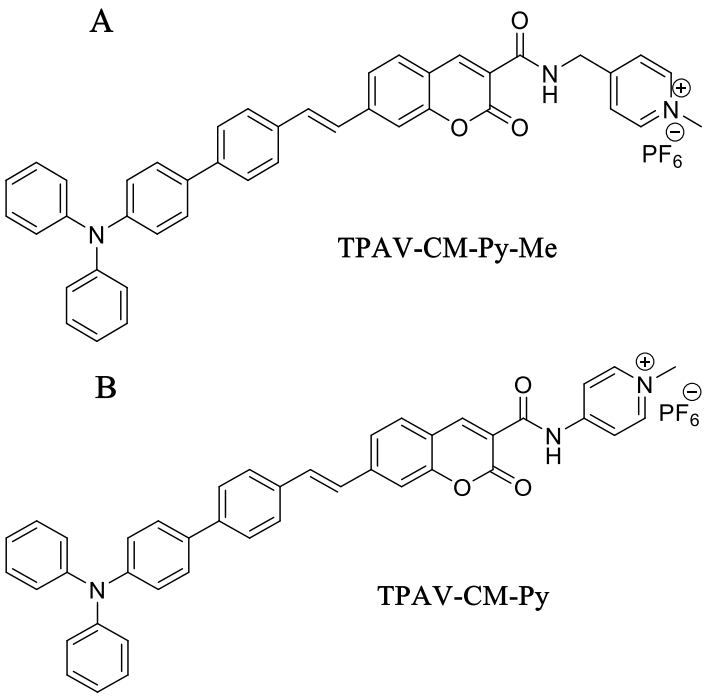

Figure 2.1. (A and B) represent the molecular structures of TPAV-CM-Py-Me and TPAV-CM-Py photosensitizers

2.4. Synthesis of TPAV-CM-Py-Me

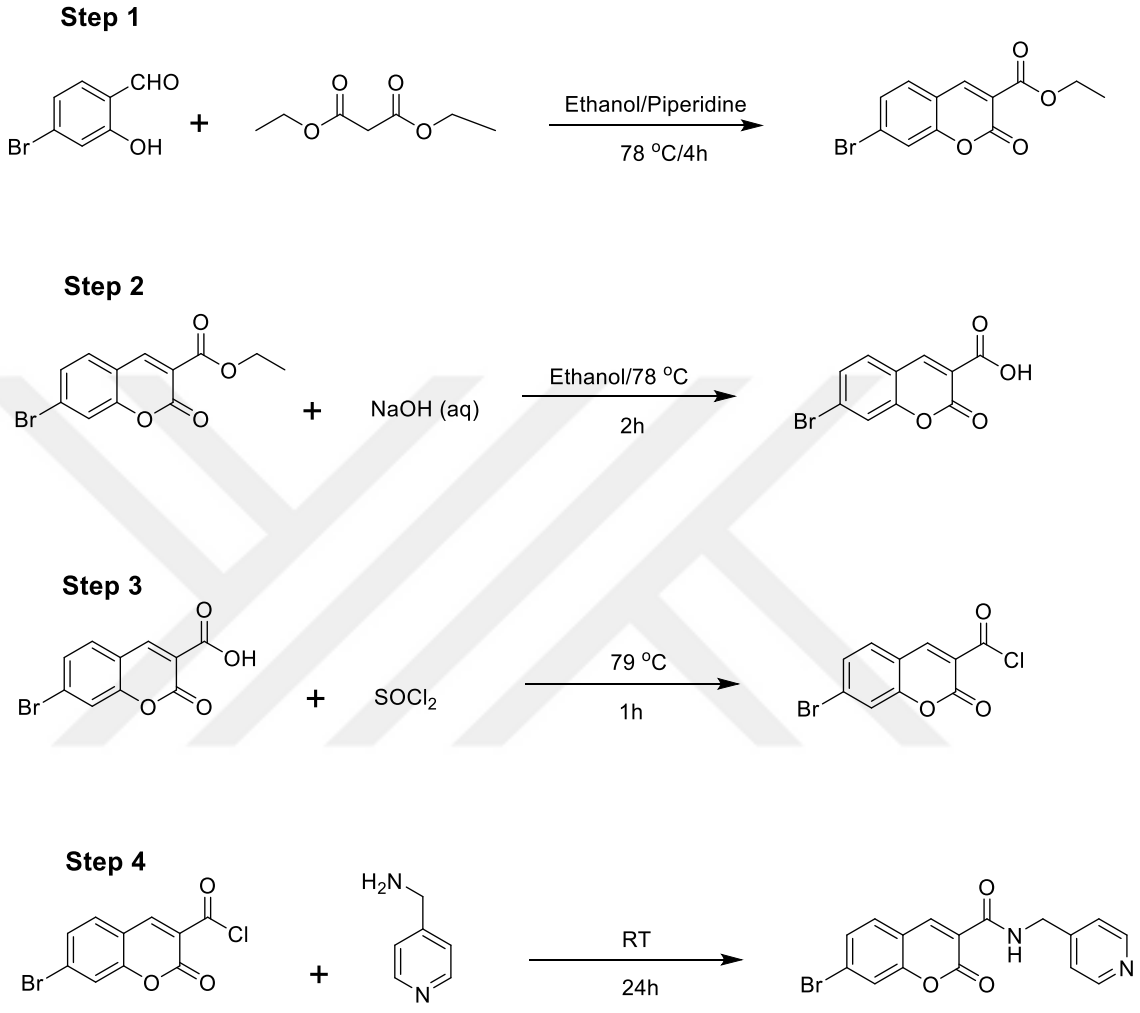

Scheme 2.1. Synthesis of TPAV-CM-Py-Me photosensitizers.

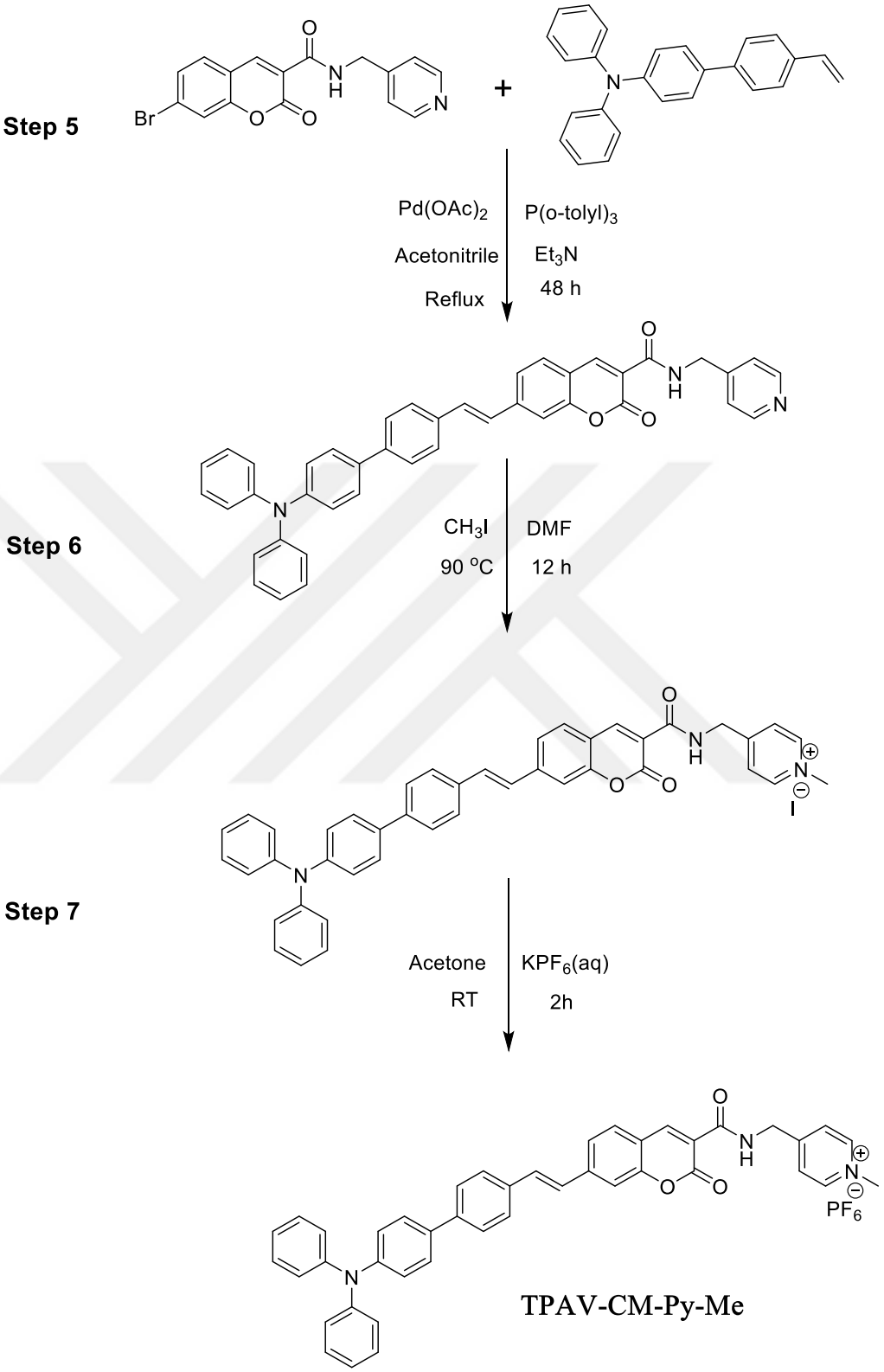

Scheme 2.2. Synthesis of TPAV-CM-Py-Me photosensitizers.

2.4.1. Synthesis route of TPAV-CM-Py-Me Photosensitizers

2.4.1.1. Synthesis of ethyl 7-bromo-2-oxo-2H-chromene-3-carboxylate

4-Bromo-2-hydroxybenzaldehyde (0.5 g, 2.487 mmol), ethyl acetoacetate (0.486 g, 3.731 mmol), and piperidine (2.487 mmol) were added to 10 mL of absolute ethanol, and the resulting mixture was refluxed for 4 hours. After cooling the mixture to room temperature, a yellow precipitate (0.38 g) was obtained, which was vacuum filtered, washed with cold ethanol, and dried under vacuum overnight (yield:70%). ^{1}H-NMR (DMSO-*d6*, 400 MHz) δ/ppm: 1.31 (t, *J* = 8 Hz, 3H), 4.30 (m, 2H), 7.60 (d, *J* = 8 Hz, 1H), 7.76 (s, 1H), 7.85 (d, *J* = 8 Hz, 1H), 8.74 (s, 1H).

2.4.1.2. Synthesis of 7-bromo-2-oxo-2H-chromene-3-carboxylic acid

10% NaOH aqueous solution mixed with ethyl 7-bromo-2-oxo-2H-chromene-3-carboxylate, and thereafter 15 mL ethanol absolute was added. Reaction mixture refluxed for 2 hours. Thereafter, ethanol was removed under vacuum and the resulting solution was treated with 6M solution of HCl to bring the pH to 2. The resulting precipitate (0.35 g) was collected through filtration and washed with water and dried under vacuum overnight (yield: 91.7%)**.** which was used for the next step without further purification and characterization.

2.4.1.3. Synthesis of 7-bromo-2-oxo-2H-chromene-3-carbonyl chloride

7-bromo-2-oxo-2H-chromene-3-carboxylic acid (0.35 mg, 0.0013 mmol) was added to thionyl chloride (2 mL) and refluxed the reaction mixture at 76^{O}C for 1 h. Thereafter, thionyl chloride was removed via a rotary evaporator to get solid white color powder (0.276 g), which was dried under vacuum for 1 hour and freshly used for the next step without further characterization and purification.

2.4.1.4. Synthesis of 7-methyl-2-oxo-N-(pyridin-4-yl)-2H-chromene-3-carboxamide

7-bromo-2-oxo-2H-chromene-3-carbonyl chloride (0.3 3g, 1.0435 mmol) and 15 mL dichloromethane were added to the flask and then purged with nitrogen gas. Sonicated under nitrogen gas to get it dissolved. On the other hand, with pyridin-4-yl methanamine (0.124 g, 1.15 mmol) or 0.117 ml of triethyl amine (0.127 g, 1.252 mmol) added in DCM

(6 mL), the reaction mixture was injected dropwise, which on the first contact produced HCl fumes with the brown and white color. Placed that reaction overnight reflux at room temperature. Obtained white precipitate, which was filtered under vacuum, washed sequentially with DCM, and dried under vacuum (yield:78%).^{1}H-NMR (DMSO-*d6*, 400 MHz) δ/ppm: 4.56 (d, *J* = 8 Hz, 2H), 7.32 (d, *J* = 4 Hz, 2H), 7.65 (d, *J* = 8 Hz, 1H), 7.86 (s, 1H), 7.92 (d, *J* = 8 Hz, 1H), 8.50 (d, *J* = 8 Hz, 2H), 8.85 (s, 1H), 9.21 (t, *J* = 4 Hz, 1H).

2.4.1.5. Synthesis of (E)-7-(2-(4'-(diphenylamino)-[1,1'-biphenyl]-4-yl) vinyl)-2-oxo-N-(pyridin-4-yl)-2H-chromene-3-carboxamide

7-methyl-2-oxo-N-(pyridin-4-yl)-2H-chromene-3-carboxamide (0.175 g, 0.507 mmol), N,N-diphenyl-4'-vinyl- [1,1'-biphenyl]-4-amine (0.158 g, 0.406 mmol), palladium(II) acetate (0.0114 g, 0.0507 mmol), tri(o-tolyl)phosphine (0.031 g, 0.1014 mmol), and Triethylamine (0.721 g, 7.098 mmol or 1 mL) were combined in a Schlenk flask and degassed multiple times. Subsequently, 4.0 mL of absolute ethanol, 14.0 mL of toluene, and 2.0 mL of deionized water were added to the flask. The resulting mixture was stirred under nitrogen at 90°C for 12 hours. The reaction's progress was monitored by thin-layer chromatography. After completion, the reaction mixture was cooled to room temperature and extracted with dichloromethane. The organic phase was dried over anhydrous Na_2SO_4, filtered, and concentrated using a rotary evaporator. The crude product was purified by column chromatography using a 2:1 (vol/vol) mixture of ethyl acetate and n-hexane. The purified product (0.183 g) was dried under vacuum overnight (Yield:68%). ^{1}H-NMR (DMSO-d6, 400 MHz): δ/ppm 4.58 (s, 2H), 7.06 (m, 8H), 7.36 (m, 7H), 7.64 (m, 9H), 7.95 (d, *J* = 8 Hz, 9H), 8.51 (d, *J* = 8 Hz, 2H), 8.83 (s, 1H), 9.22 (s, 1H).

2.4.1.6. Synthesis of E)-4-(7-(2-(4'-(diphenylamino)- [1,1'-biphenyl]-4-yl) vinyl)-2-oxo-2H-chromene-3-carboxamido)-1-methylpyridin-1-ium

(E)-7-(2-(4'-(diphenylamino)-[1,1'-biphenyl]-4-yl)vinyl)-2-oxo-N-(pyridin-4-yl)-2H-chromene-3-carboxamide (0.1 g, 0.1635 mmol) was mixed with iodomethane (0.462 g, 3.27 mmol or 250 μL) in the presence of 15 mL of acetonitrile as solvent. The mixture was refluxed at 90°C overnight. Upon completion of the reaction, the solvent was evaporated using a rotary evaporator. The remaining residue formed a crimson-red precipitate in the presence of ethyl acetate, which was collected by vacuum filtration. The

crimson red precipitate was obtained as the product and used for the next step without further characterization or purification (yield:54%).

2.4.1.7. Ion Exchange

(E)-4-(7-(2-(4'-(diphenylamino)-[1,1'-biphenyl]-4-yl)vinyl)-2-oxo-2H-chromene-3carboxamido)-1-methylpyridin-1-ium (0.85 g, 1.477 mmol) was mixed with 5 mL of acetone, and a 6 mL saturated solution of potassium hexafluorophosphate was added dropwise. The mixture was stirred for 2 hours at room temperature. The resulting precipitate was collected by filtration, washed with water, and dried under vacuum overnight. ^{1}H-NMR (DMSO-*d6*, 400 MHz) δ/ppm: 4.29 (s, 3H), 4.81 (d, *J* = 8 Hz, 2H), 7.07 (m, 8H), 7.38 (m, 6H), 7.70 (m, 9H), 8.00 (m, 6H), 8.86 (m, 2H), 9.45 (t, *J* = 8 Hz, 1H). ^{13}CNMR (100 MHz, DMSO-*d*6): δ/ppm= 42.79, 47.67, 113.66, 117.92, 118.03, 123.58, 123.85, 124.73, 125.69, 126.90, 127.09, 127.97, 128.19, 130.10, 131.06, 133.14, 133.59, 135.44, 140.13, 144.11, 145.49, 147.42, 147.92, 147.92, 150.48, 155.29, 159.40, 162.70. HRMS (ESI): (m/z) Calculated for $C_{43}H_{34}N_3O_3^+$ [M] $^+$ 640.2625 found 640.2584.

2.5. Synthesis of TPAV-CM- Py

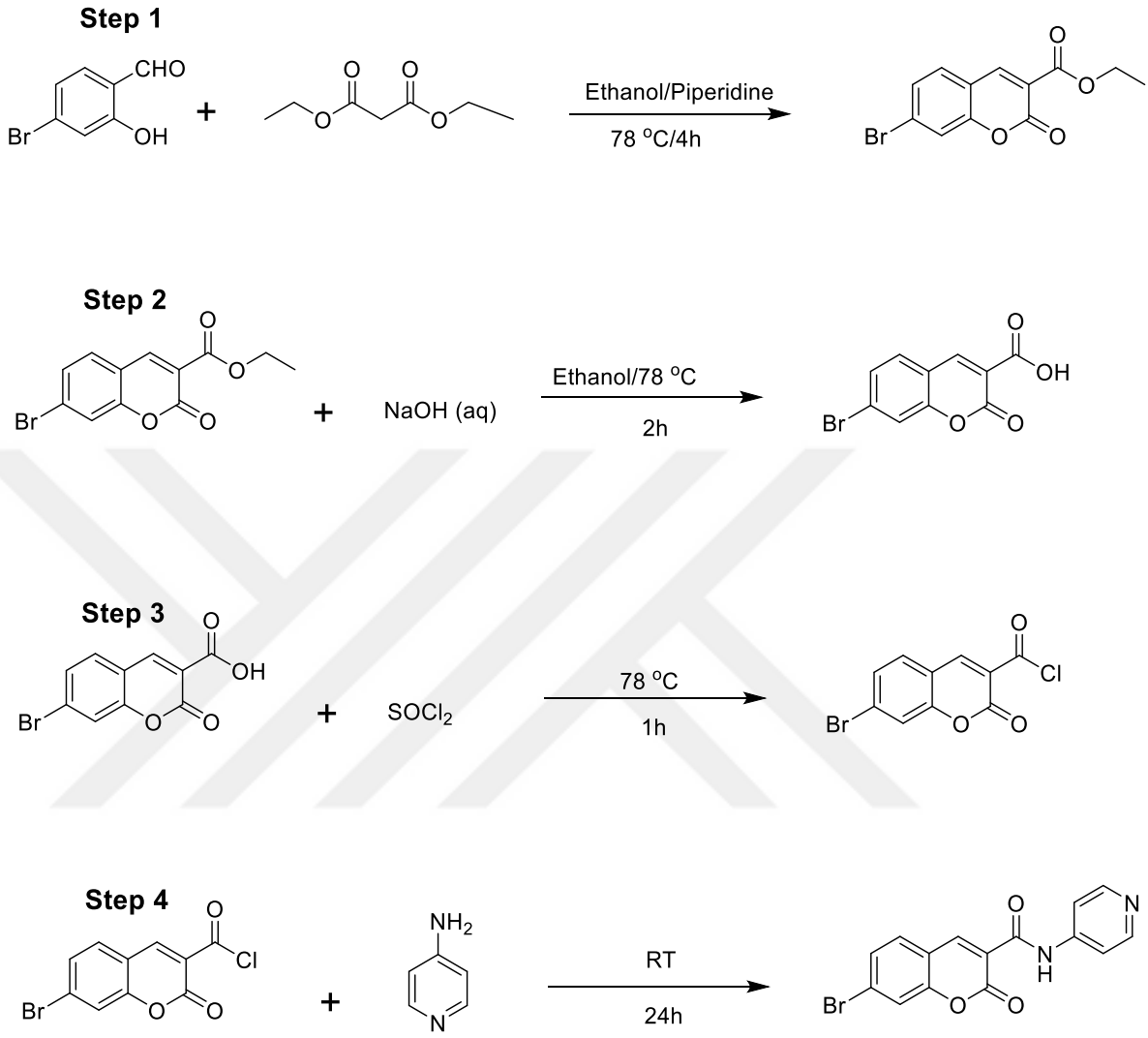

Scheme 2.3. Synthesis of TPAV-CM-Py photosensitizers.

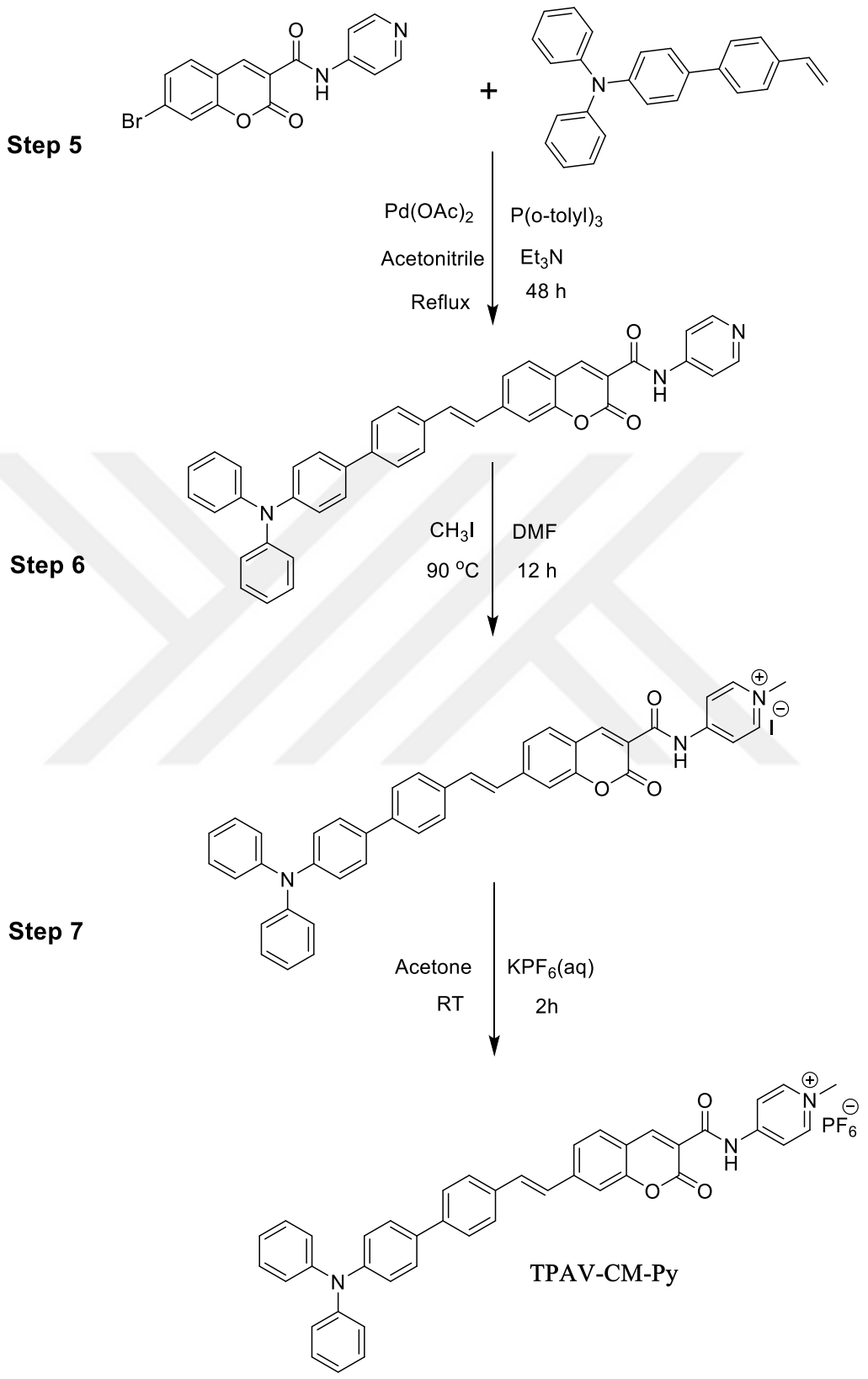

Scheme 2.4. Synthesis of TPAV-CM-Py photosensitizers.

2.5.1. Synthesis of TPAV-CM-Py Photosensitizers

The synthesis methodology for TPAV-CM-Py photosensitizers is the same as that for TPAV-CM-Py-Me, as mentioned in schemes 2.1 and 2.2. It was prepared according to the protocol adopted for TPAV-CM-PY-ME. The synthetic scheme and the reaction conditions are given below in Scheme 2.

Step 1 to step 3 is same as above-mentioned protocol for TPAV-CM-Py-Me.

2.5.1.1. Synthesis of 7-bromo-2-oxo-N-(pyridin-4-ylmethyl)-2H-chromene-3-carboxamide

7-bromo-2-oxo-2H-chromene-3-carbonyl chloride (0.3 g, 1.0435 mmol) and dichloromethane were added in a flask, then purged with nitrogen gas, sonicated under a nitrogen gas balloon to get it dissolved. On the other hand, pyridin-4-amine (0.124 g, 1.15 mmol) or 0.117 ml, Triethylamine (0.127 g, 1.252 mmol) or 0.175mL added in DCM (6 mL), the reaction mixture was injected dropwise, which on the first contact produced HCl fumes with the brown and white color. Placed that reaction overnight reflux on room temperature. Obtained white precipitate (0.234 g), which was filtered under vacuum, washed sequentially with DCM, and dried under vacuum (yield: 74.6%). ^{1}H-NMR (DMSO-*d6*, 400 MHz) δ/ppm: 7.70 (m, 3H), 7.93 (m, 2H), 8.51 (d, *J* = 4 Hz, 2H), 8.88 (s, 1H), 10.85 (s, 1H).

2.5.1.2. Synthesis of (E)-7-(2-(4'-(diphenylamino)-[1,1'-biphenyl]-4-yl)vinyl)-2-oxo-N-(pyridin-4-yl)-2H-chromene-3-carboxamide

I7-methyl-2-oxo-N-(pyridin-4-yl)-2H-chromene-3-carboxamide (0.183 g, 0.567 mmol), N,N-diphenyl-4'-vinyl-[1,1'-biphenyl]-4-amine (0.15 g, 0.406 mmol), palladium (II) acetate (0.0114 g, 0.0507 mmol), tri(o-tolyl)phosphine (0.031 g , 0.1014 mmol), triethyl amine (0.721 g, 7.098 mmol), were mixed in a Schlenk flask and degassed multiple times. Thereafter, 4.0 mL absolute ethanol, 14.0 mL toluene, and 2.0 mL deionized water were injected into the Schlenk flask. The resulting mixture was stirred under nitrogen at 90°C for 12 hours. The reaction's progress was monitored by thin-layer chromatography. After completion, the reaction mixture was cooled to room temperature and extracted with dichloromethane. The organic phase was dried over anhydrous Na_2SO_4, filtered, and

concentrated using a rotary evaporator. The crude product was purified by column chromatography using a 2:1 (vol/vol) mixture of ethyl acetate and n-hexane. The obtained product was dried under vacuum overnight (0.138 g, yield:68%). ^{1}H-NMR (DMSO-*d6*, 400 MHz) δ/ppm: 7.07 (d, 8H), 7.36 (t, 6H), 7.98 (s, 10H), 8.52 (s, 2H), 8.87 (s, 1H), 10.82 (s, 1H).

2.5.1.3. Synthesis of (E)-4-(7-(2-(4'-(diphenylamino)- [1,1'-biphenyl]-4-yl)vinyl)- 2-oxo-2H-chromene-3-carboxamido)- 1-methylpyridin-1-ium

(E)-7-(2-(4'-(diphenylamino)-[1,1'-biphenyl]-4-yl)vinyl)-2-oxo-N-(pyridin-4-yl)-2H-chromene-3-carboxamide (0.1 g, 0.1635 mmol) mixed with iodomethane (0.462 g, 3.27 mmol) or 250 μL will be used in the presence of the solvent acetonitrile (15 mL) refluxed at 90 °C overnight. After the completion of the reaction, the solvent gets evaporated by a rotary evaporator. The remaining were settled down as red colored precipitate in the presence of ethyl acetate. which filtration using a vacuum collects further. Crimson red color precipitate was formed 0.63 g (yield: 42%). The product formed used for the next step without any further characterization and purification.

2.5.1.4. Ion Exchange

(E)-4-(7-(2-(4'-(diphenylamino)-[1,1'-biphenyl]-4-yl)vinyl)-2-oxo-2H-chromene-3carboxamido)-1-methylpyridin-1-ium (0.1 g, 1254 mmol) mixed with 5 ml acetone and 6 ml of saturated solution of potassium hexafluorophosphate. Stir the mixture for 2h at room temperature. The resulting precipitate was collected through filtration and washed with water, and dried under vacuum overnight**.** ^{1}H-NMR (DMSO-*d6*, 400 MHz) δ/ppm: 4.18 (s, 3H), 7.07 (m, 8H), 7.37 (m, 5H), 7.69 (m, 9H), 8.01 (d, *J* = 8 Hz, 1H), 8.28 (d, *J* = 8 Hz, 2H), 8.77 (d, *J* = 8 Hz, 2H), 8.93 (s, 1H), 11.59 (s, 1H). ^{13}CNMR (100 MHz, DMSO-*d*6): δ/ppm= 46.94, 100.07, 113.98, 116.27, 117.81, 117.89, 123.52, 123.87, 124.75, 124.10, 124.75, 126.85, 126.90, 127.95, 128.26, 130.10, 131.46, 133.41, 133.64, 135.31, 140.19, 144.96, 146.62, 147.41, 147.48, 149.35, 149.44, 150.99, 155.35, 160.43, 162.80. HRMS (ESI): (m/z) Calculated for $C_{42}H_{32}N_3O_3^+$ [M] $^+$ 626.2438 found 626.2419.

2.6. Cytotoxicity study

To determine the light/dark field cytotoxicity of the prepared TPAV-CM-Py-Me and TPAV-CM-Py, cell viability was evaluated on MCF-7 breast cancer cell line by MTT

assay. Briefly, MCF-7 cells in 100 µl complete DMEM culture medium (Dulbecco's Modified Eagle's Medium, High Glucose) supplemented with 10% FBS (Fetal Bovine Serum) were transferred to a 96-well plate and incubated at 37°C with moisture containing 5% CO_2 for 24 h (5 x 10^3/well). The cells were then treated with TPAV-CM-PY-Me and TPAV-CM-Py at different concentrations (0–5 µM/mL) for 24h. To perform a comparative analysis of dark field toxicity and light field toxicity, two different plates were prepared under the same conditions. One of the plates was exposed to white light for 30 minutes, while the other was incubated in a dark environment during this time. Then, 20 µl of MTT at a concentration of 5 mg/mL was added to each well and incubated for 4 h. Following the removal of the solution from each well, 100 µL of DMSO was added. The absorbance of each well was then measured at 570/640 nm with a microplate reader (Multiskan FC, Thermo-Scientific, USA), and the cell viability was calculated using the given formula.

Cell viability (%) = $(OD_{Sample} - OD_{Blank}) / (OD_{Cont\ Control} - OD_{Blank}) \times 100\%$

2.7. In Vitro Analysis

A confocal plate was used for live-cell imaging of the prepared molecules and 5 x 10^3 MCF-7 cells per well were seeded in a similar procedure as in cytotoxicity assays. After 24 h incubation, TPAV-CM-Py-Me and TPAV-CM-Py (10 µmol/L) were added to the wells with fresh media. After 2 h incubation, the media was removed, and the cells were washed with PBS twice. After adding a culture medium containing Hoechst-33342 at a concentration of 1µM/mL, the cells were incubated for 5 minutes, washed with PBS, and examined using a confocal microscope.

2.8. Singlet Oxygen Generation

2.8.1. Singlet Oxygen Detection in Aqueous Medium (Extracellular ROS Generation)

Extracellular ROS generation was evaluated by ABDA, which is a standard commercial indicator for $^1O_2$ detection. In detail, aqueous solutions of TPAV-CM-Py-Me (20 µM) and ABDA (150 µM) were mixed in a 1:1 ratio to get 10 µM and 75 µM final working solution concentrations of TPAV-CM-Py-Me and ABDA, respectively. The mixture was

irradiated under white light (LED Lamp: 15 watt) for 10-180 seconds, The decomposition of ABDA at 378 nm was studied via a UV-visible spectrophotometer. To ensure the effectiveness of our synthesized photosensitizer, commercial PSs Rose Bengal (10 μM) were used using the same procedure as for TPAV-CM-Py-Me, and the decomposition of ABDA was studied at 378 nm. Same procedure was followed of TPAV-CM-Py extracellular singlet oxygen generation experiment.

2.8.2. Singlet Oxygen Detection in Cancer Cells (Intracellular ROS Generation)

To determine the ability of the designed TPAV-CM -Py-Me and TPAV-CM-Py to produce reactive oxygen species (ROS), the MCF-7 cells were cultured in a 96-well plate with 5 x 10^3 cells and incubated overnight. After incubation, the culture medium containing different concentrations of molecules was replaced. After 2 h incubation, the medium was removed and washed twice with PBS. Medium containing 2′,7′-Dichlorofluorescein diacetate (DCFH-DA) at a concentration of 20 μM/mL was added and incubated for 30 min. Afterward, the existing medium was replaced with a fresh medium. The light was exposed (LED Lamp: 15 watt) for 30-40 min, and images were taken using a confocal microscope.

CHAPTER 3

RESULTS AND DISCUSSION

3.1. Characterization of TPAV-CM-Py-Me and TPAV-CM-Py

TPAV-CM-Py-Me and TPAV-CM-Py were designed and synthesized successfully by Heck cross-coupling reaction and the synthetic protocols are shown in (Scheme 2.1-2.4). The chemical structures of the intermediates and final products were characterized by nuclear magnetic resonance (NMR) spectroscopy and high-resolution mass spectrometry (HRMS). The NMR results for TPAV-CM-Py-Me are shown in Figure 3.1 and 3.2, while for TPAV-CM-Py are shown in Figure 3.4 and 3.5. HRMS results for TPAV-CM-Py-Me and TPAV-CM-Py are shown in Figures 3.3 and 3.6, respectively.

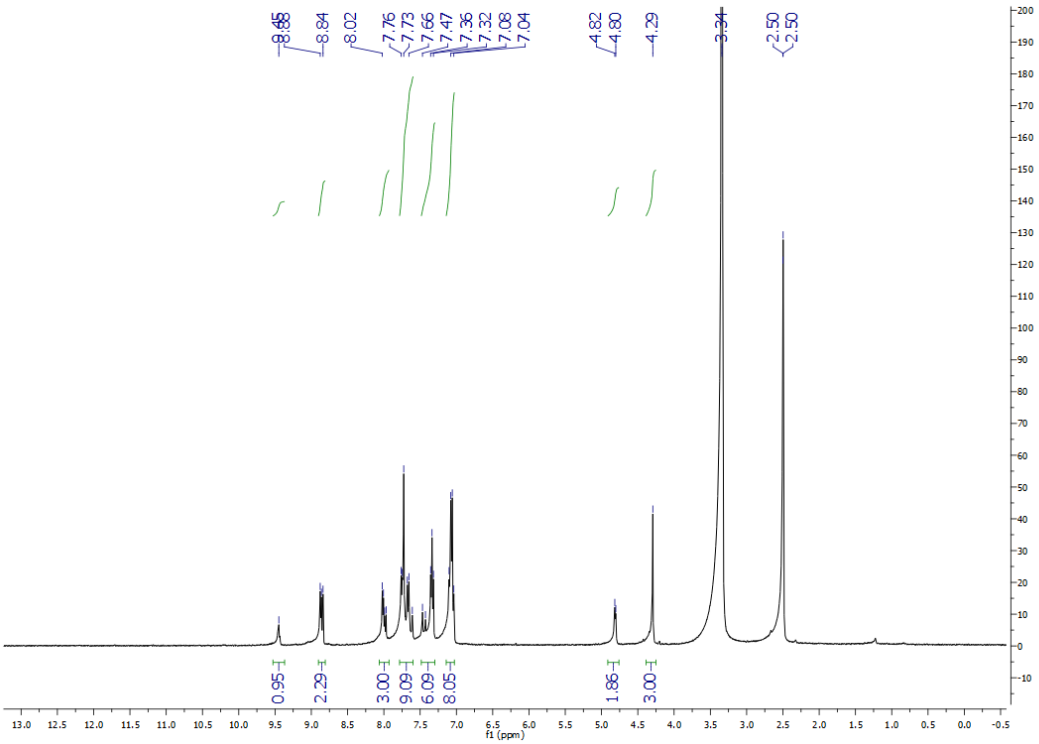

Figure 3.1. ^{1}H-NMR spectrum of TPAV-CM-Py-Me

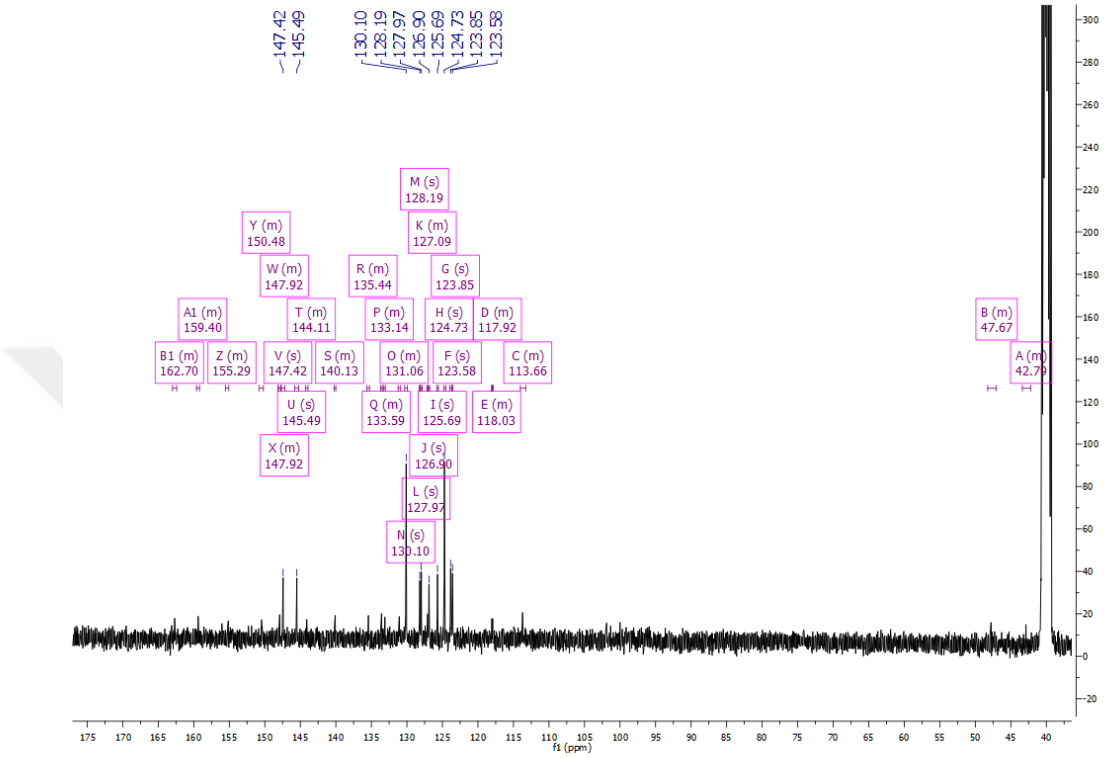

Figure 3.2. ^{13}C-NMR spectrum of TPAV-CM-Py-Me

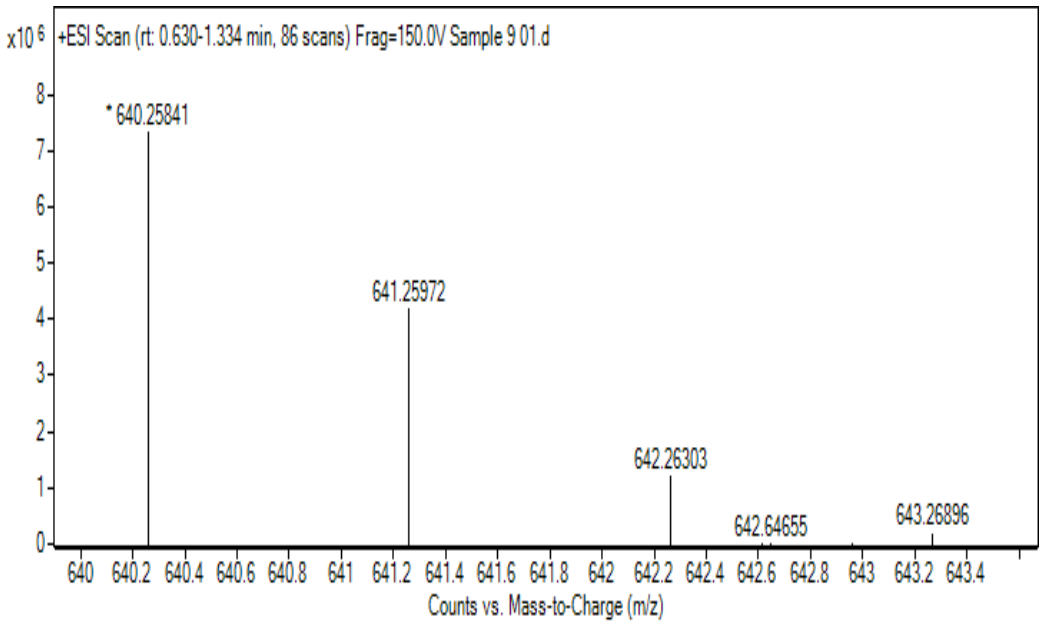

Figure 3.3. High resolution mass spectrum of TPAV-CM-Py-Me

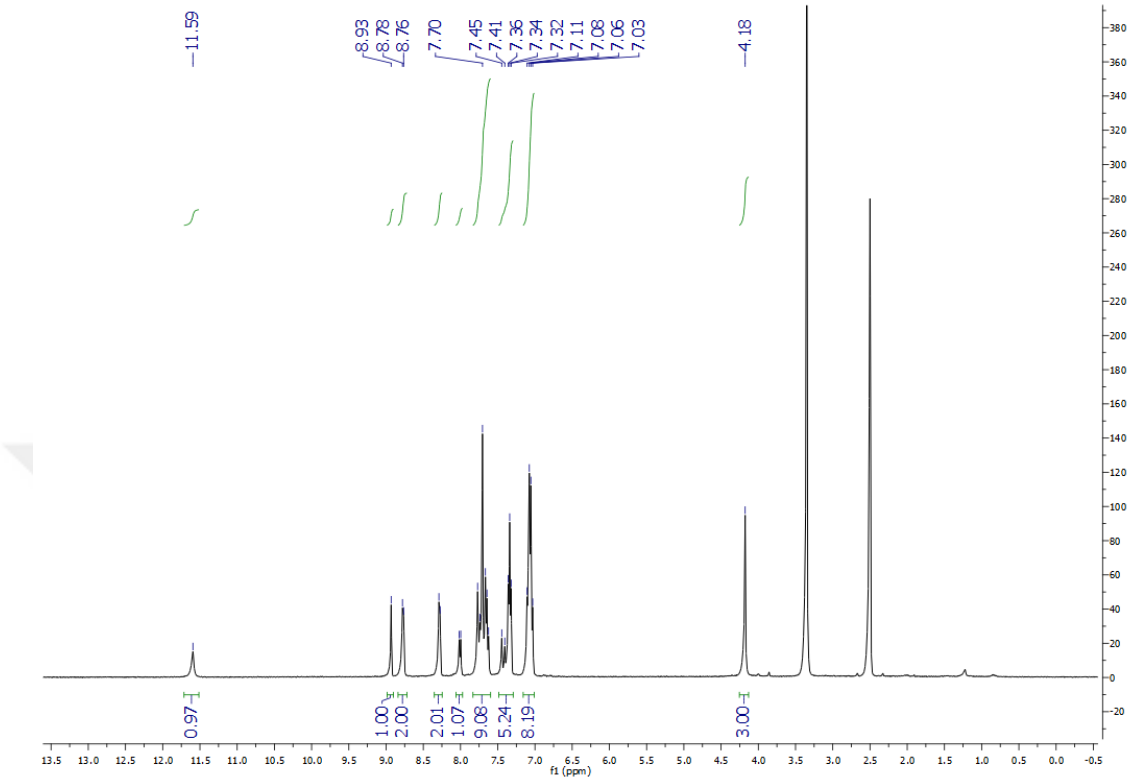

Figure 3.4. [1]H-NMR spectrum of TPAV-CM-Py

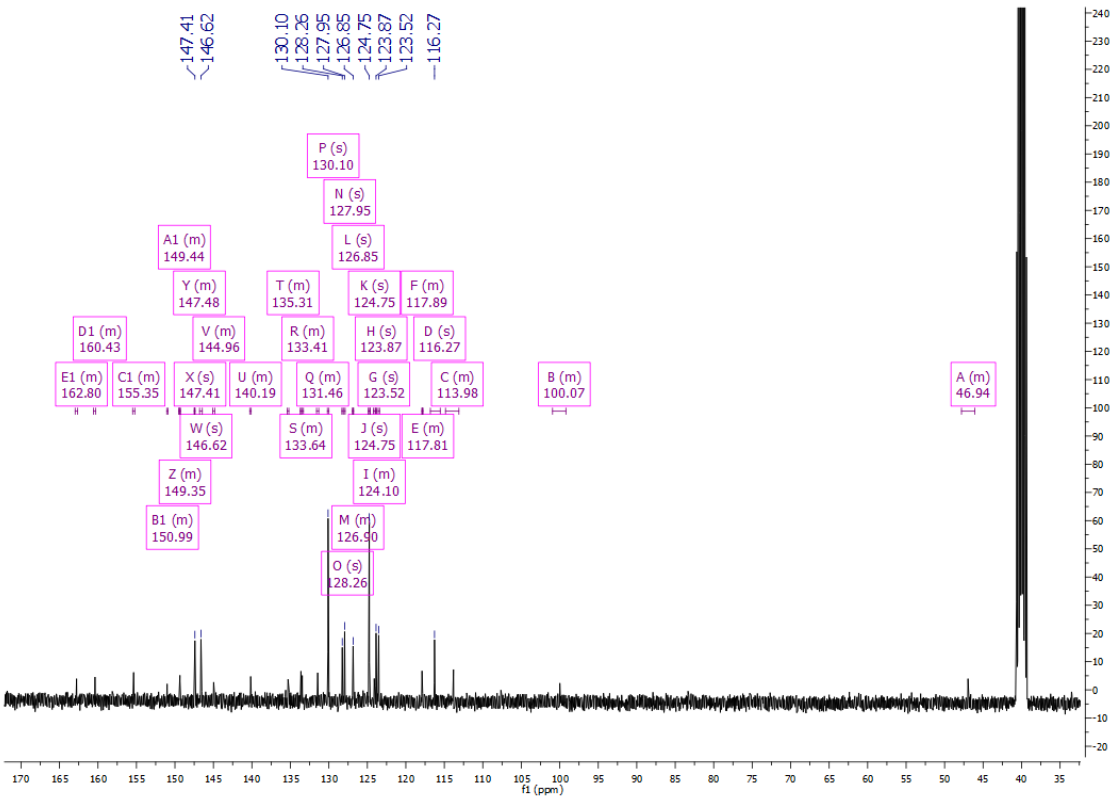

Figure 3.5. ^{13}C-NMR spectrum of TPAV-CM-Py

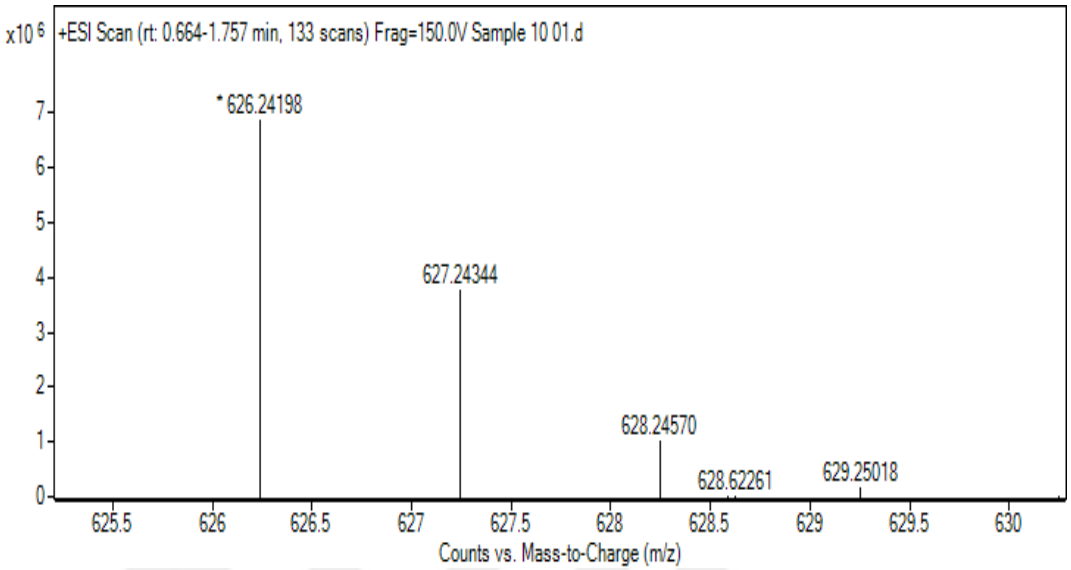

Figure 3.6. High resolution mass spectrum of TPAV-CM-Py

3.2. Photophysical Property

Photophysical properties of the designed AIEgens were studied using fluorescence and ultraviolet-visible (UV-vis) spectroscopy. The UV-vis spectra of TPAV-CM-Py-Me and TPAV-CM-Py were obtained in chloroform and the results are shown in Figures 3.8 (A) (TPAV-CM-Py-Me) and 3.9 (A) (TPAV-CM-Py), which exhibit the absorption maxima at 434 nm and 442 nm, respectively. For fluorescence emission spectra, we tried different solvents (Figure 3.7) to choose the best solvent, as AIE molecules are normally non-fluorescent or weakly fluorescent in their solution forms. One can see Figure 3.7 (B) that TPAV-CM-Py-Me shows best fluorescence in chloroform, while in the other common organic solvents, such as acetone, dichloromethane, ethyl acetate, and tetrahydrofuran, it is either non-fluorescent or weakly fluorescent. On the other hand, TPAV-CM-Py (Figure 3.7 D) exhibits intense fluorescence in tetrahydrofuran, while in the other common organic solvents, such as chloroform, acetone, dichloromethane, and ethyl acetate, it is either non-fluorescent or weakly fluorescent. Therefore, chloroform and tetrahydrofuran were chosen to record the fluorescence emission spectra for TPAV-CM-Py-Me and TPAV-CM-Py, respectively. One can see from Figure 3.8 (B) that TPAV-CM-Py-Me exhibits emission maxima at 640 nm, while TPAV-CM-Py 3.9 (B) shows the maximum

emission peak at 553 nm. The polarity index of THF is lower than chloroform, because TPAV-CM-Py exhibited blue shift owing to its donor-acceptor nature. The results revealed that synthesized compounds had strong absorption intensity and emission intensity in the visible region, thus indicating that the synthesized compounds have good fluorescence properties.

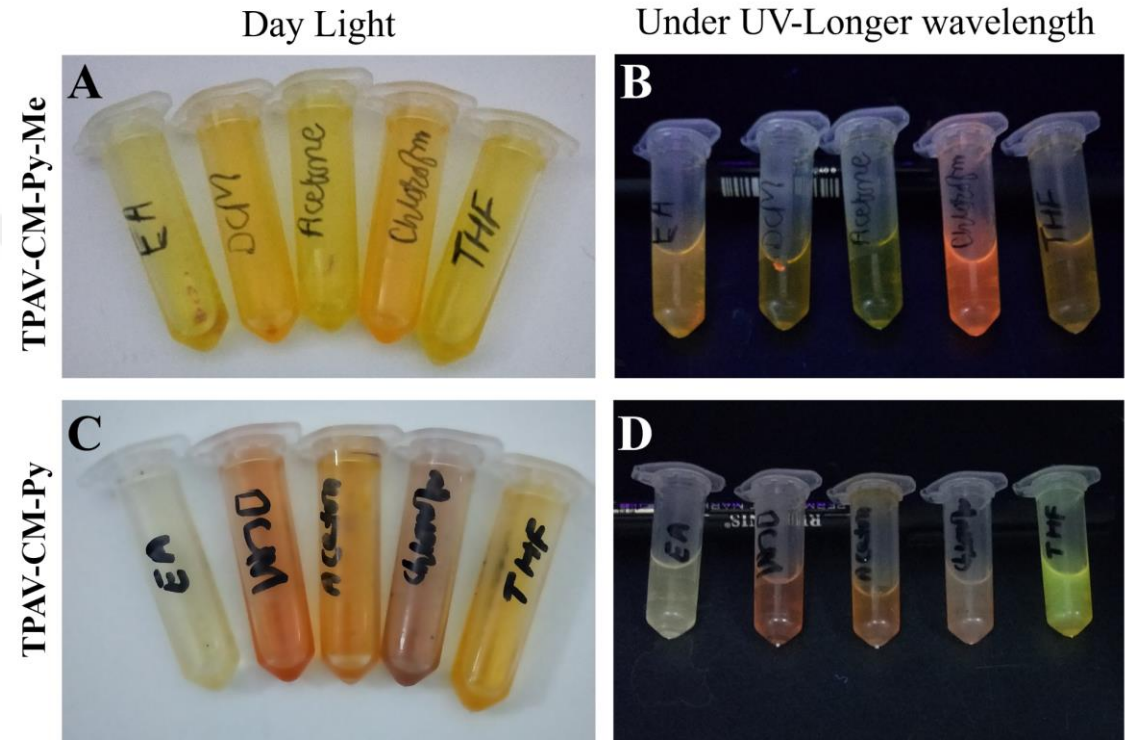

Figure 3.7. Analysis of TPAV-CM-Py-Me and TPAV-CM-Py in different solvents under day light and UV-Lamp

To analyze the AIE properties of our synthesized photosensitizer, the fractions of DMSO/ Toluene were studied. In pure DMSO no fluorescence was observed, with the fraction ranging from 10 to 99%. However, the AIE phenomenon was observed significantly when fraction of toluene was increased from 90 to 99%, as presented below in Figure 3.8 (C and D). TPAV-CM-Py-Me showed maximum fluorescence at 99% in DMSO/Toluene fraction (based on volume). While TPAV-CM-Py showed maximum fluorescence at 90% in DMSO/Toluene fraction (based on volume) as shown in Figure 3.9 (C and D). The results indicate that the Stokes shifts for TPAV-CM-Py-Me and TPAV-CM-Py are approximately 212 nm and 110 nm, respectively. These large Stokes shifts values suggested that the compounds can be used as biomedical applications to prevent self-quenching.

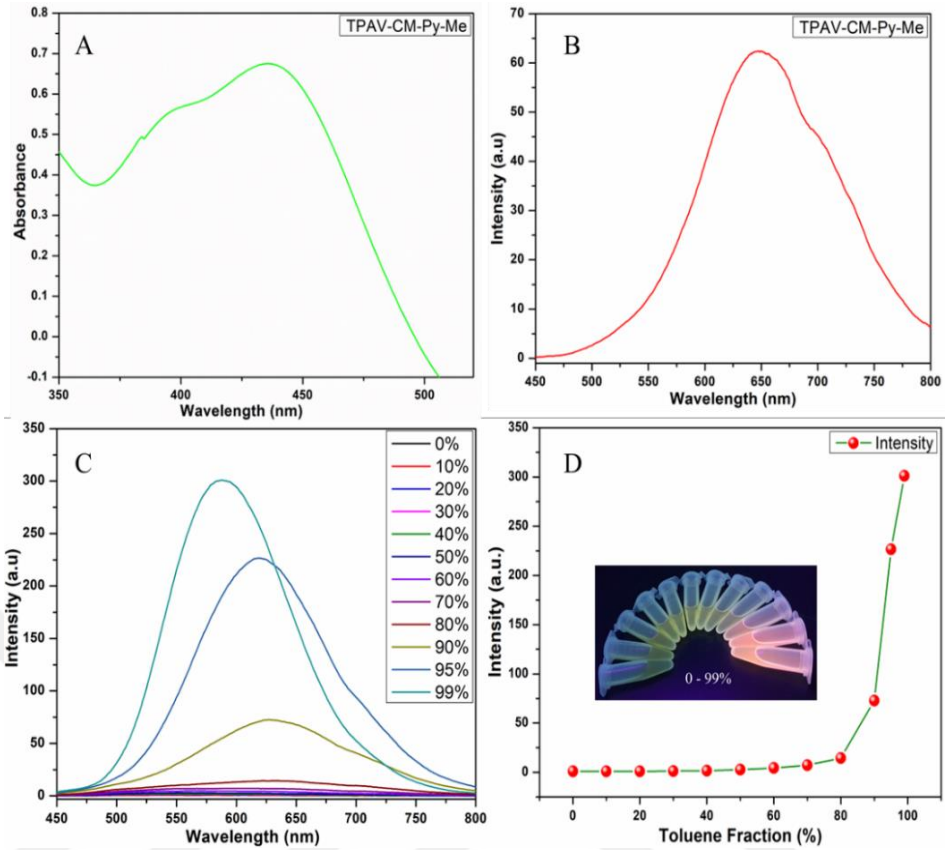

Figure 3.8. TPAV-CM-Py-Me: (A) Absorption spectrum in chloroform, (B) emission spectrum in chloroform. (C) Emission FL spectra of TPAV-CM-Py-Me in the DMSO/toluene mixtures with different toluene fractions (based on the volume). (D) Plot of the TPAV-CM-Py-Me FL intensity as a function of the toluene fraction. The data were extracted from the maximal FL intensities of the curves. The concentration of TPAV-CM-Py-Me was 10^{-4}M

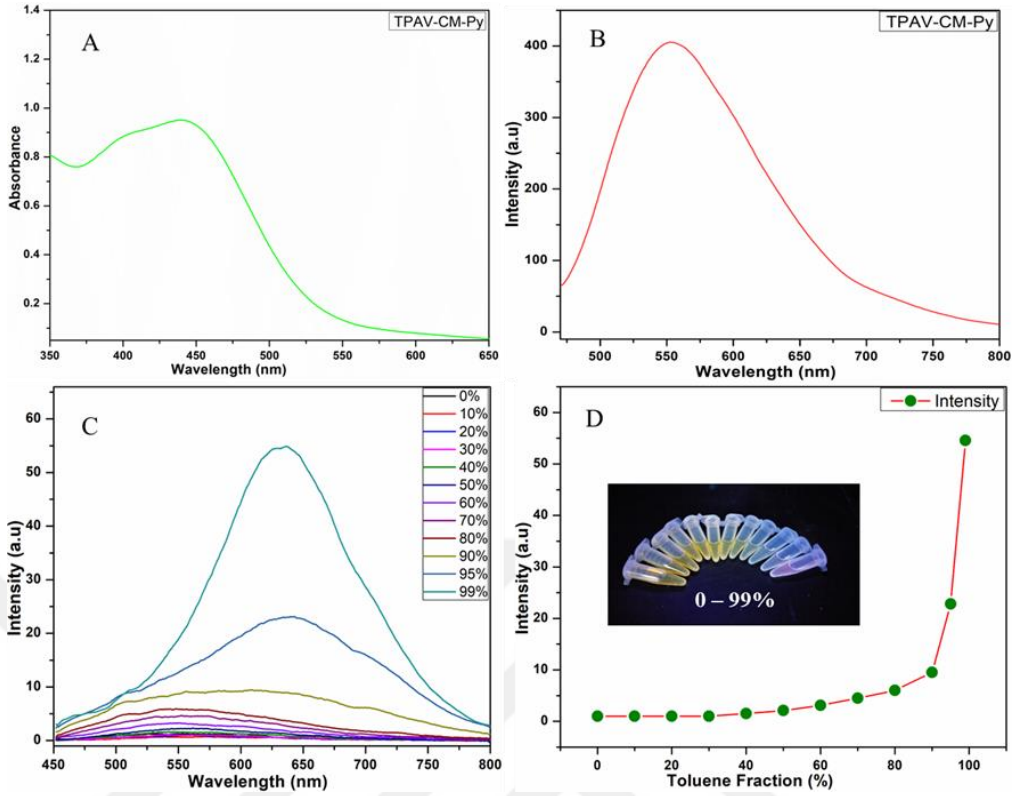

Figure 3.9. (A and B) TPAV-CM-PY has Absorption and fluorescence (FL) emission spectra of 442 nm and 553 nm, respectively. (C) Emission FL spectra of TPAV-CM-Py in the DMSO/toluene mixtures with different toluene fractions (based on the volume). (D) Plot of the TPAV-CM-Py FL intensity as a function of the toluene fraction. The data were extracted from the maximal FL intensities of the curves. The concentration of TPAV-CM-Py was 10^{-4}M

3.3. Dynamic Light Scattering Characterization Results

The sizes of the aggregated molecules of TPAV-CM-Py-Me and TPAV-CM-Py were determined using the dynamic light scattering (DLS) technique. The results revealed that TPAV-CM-Py-Me has a narrow size distribution ranging from 90 to 110 nm, whereas TPAV-CM-Py exhibited a broader size distribution in the range between 10 nm and 160 nm, as shown in Figure 3.10. This result suggested that this type of size distribution is useful for biomedical applications**.**

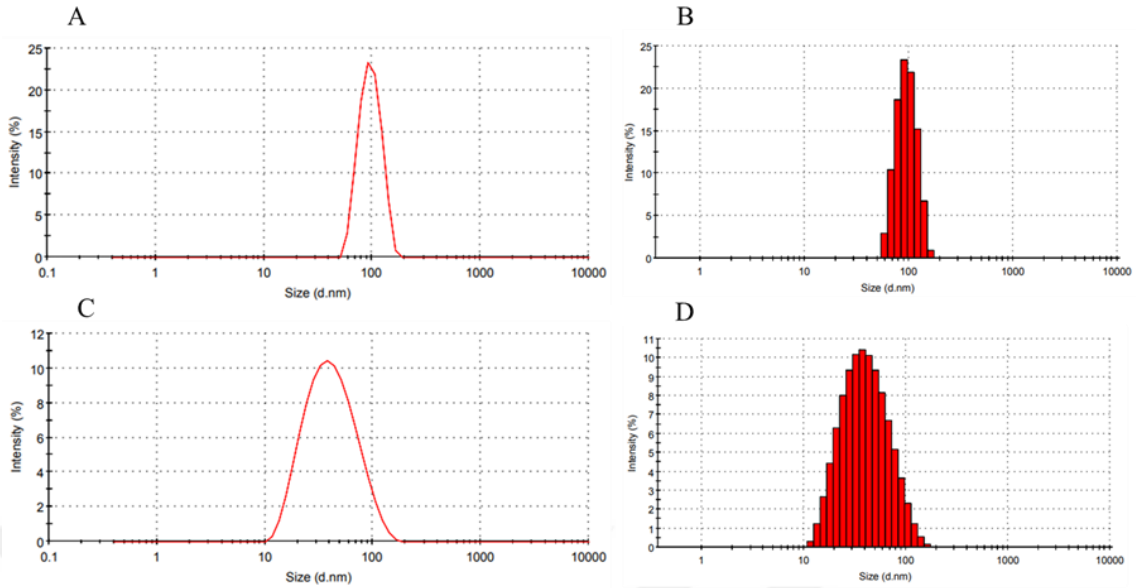

Figure 3.10. (A and B) represents the DLS analysis of TPAV-CM-Py-Me. (C and D) represent the DLS analysis of TPAV-CM-Py

3.4. SEM and STEM Characterization Results

To verify the nano-size aggregation of the synthesized molecules, scanning transmission electron microscopy (STEM) was performed. Scanning electronic microscopy (SEM) analyses were conducted to confirm the morphology of designed PSs. For these analysis, TPAV-CM-Py-Me was prepared in a solution consisting of 990 µM/mL toluene and 10 µM/mL DMSO solution of TPAV-CM-Py-Me. Similarly, TPAV-CM-Py was prepared using 900 µM/mL toluene and 100 µM/mL DMSO solution of TPAV-CM-Py. The results are depicted in Figure 3.11. STEM analysis revealed that the TPAV-CM-Py and TPAV-CM-Py-Me has both the size of 200 nm. SEM revealed the round shape morphology of synthesized PSs.

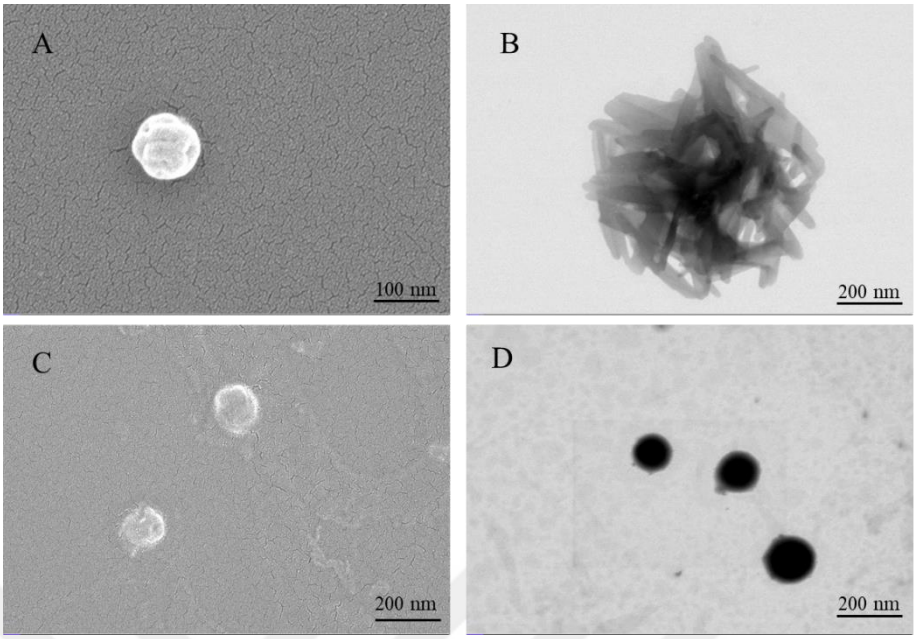

Figure 3.11. (A and B) represent the SEM and STEM results of TPAV-CM-Py-Me, respectively. (C and D) represent SEM and STEM results of TPAV-CM-Py, respectively

3.5. Light-Triggered $^1O_2$ Generation

The singlet oxygen species produced by AIE were further examined using white light (LED) as a radiation source, as its absorption wavelengths fall within the visible spectrum. The $^1O_2$ generation ability of the two AIE-PSs were assessed using a 9,10-anthracenyl-bis (methylene)-di malonic acid (ABDA) as ROS sensor. The photostability of the ABDA sensor was also examined under the white light source in Figure 3.12 (A) to prove the stability. To compare the ROS generation ability of designed AIE-PSs, a commercially available photosensitizer named Rose Bengal was used. The graph given in Figure 3.12 (B) revealed that the degradation rate of ABDA was poor in the presence of Rose Bengal.

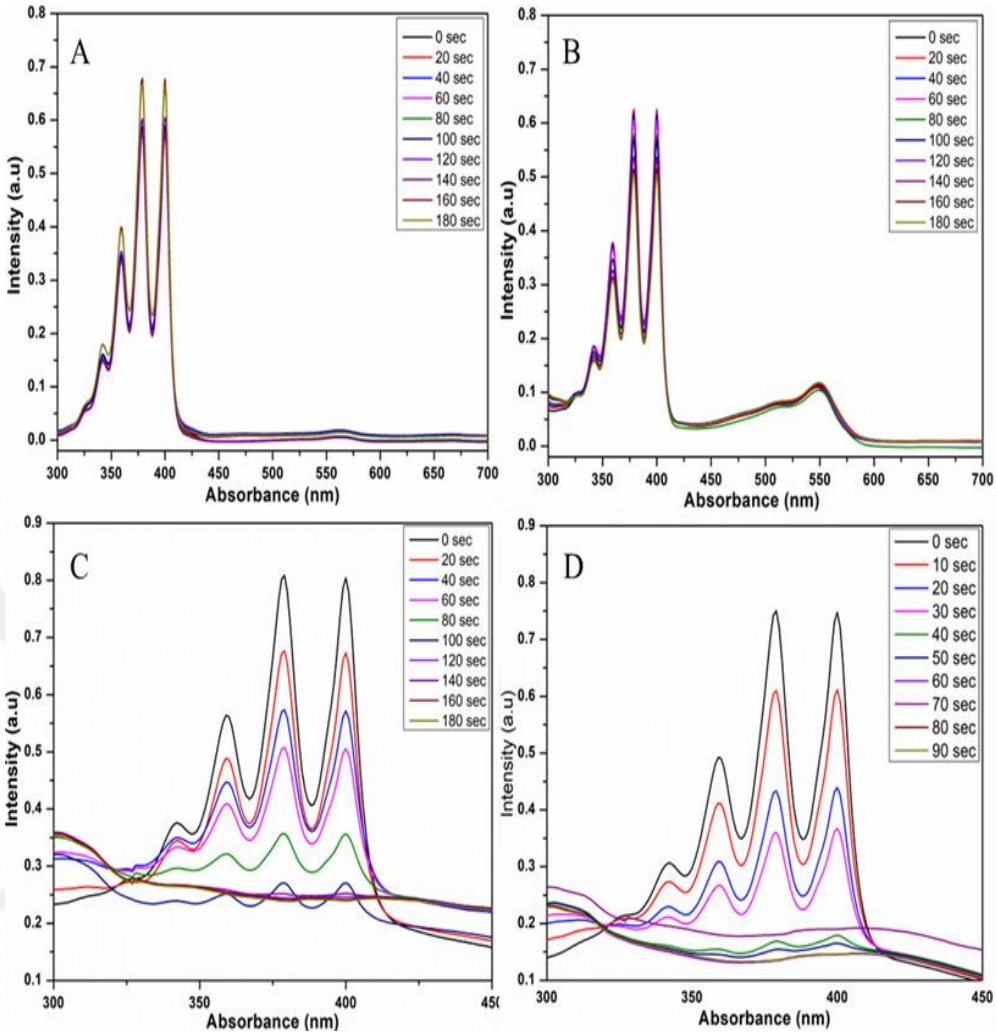

Figure 3.12. (A) Absorption spectra of ABDA in the presence of white light irradiation B) Breakdown of ABDA in the presence of Rose Bengal (C) Breakdown of ABDA in the presence of TPAV-CM-Py-Me photosensitizer with white light irradiation (D) Breakdown of ABDA in the presence of TPAV-CM-Py photosensitizer with white light irradiation

Experiments with TPAV-CM-Py-Me, TPAV-CM-Py, and Rose Bengal in the presence of ABDA were performed under the same conditions. TPAV-CM-Py-Me decomposes the ABDA in the first 120 sec, while TPAV-CM-Py decomposes the ABDA completely in the first 60 sec (Figure 3.12 C and D). The lower decomposition ability of TPAV-CM-Py-Me may be because of an extra methylene bridge near its acceptor site, while TPAV-CM-Py has higher ROS generation ability which may be due to the presence of higher conjugation in its structure as compared to TPAV-CM-Py-Me. All these results indicated that the designed PSs have excellent ability to produce ROS as than commonly used commercially available Rose Bengal.

3.6. Cell Imaging

After observing the ROS generation properties of synthesized TPAV-CM-Py-Me and TPAV-CM-Py in water, their interaction with mammalian and cancer cells was also studied.

3.6.1. Cytotoxicity Analysis

The cytotoxicity of TPAV-CM-Py-Me and TPAV-CM-Py was evaluated using the 3-(4,5-dimethyl-2-thiazolyl)-2,5-diphenyl-2H-tetrazolium bromide (MTT) assay. MCF-7 cells, a model cell line representative of breast cancer tissue, were incubated with varying concentrations (0–5 μM/mL) of TPAV-CM-Py-Me and TPAV-CM-Py for 24 h. As shown in Figure 3.5., both compounds exhibited negligible toxicity towards MCF-7 cells in the absence of light, indicating good cytocompatibility.

The photo-induced toxicity of TPAV-CM-Py-Me and TPAV-CM-Py were studied under white light irradiation (LED Lamp: 15 watt) by using MCF-7 cancer cell line and the results are demonstrated in Figure 3.13 (A and B). One can see from Figure 3.13 that after 40 minutes of intense white light irradiation, TPAV-CM-Py-Me achieved approximately 92% cancer cell eradication, whereas TPAV-CM-Py resulted in around 60% cancer cell death. AIE-PSs showed good photodynamic ablation of cancerous cells owing to their significant ROS generation. The results of dark and light toxicity are shown in Figure 3.13.

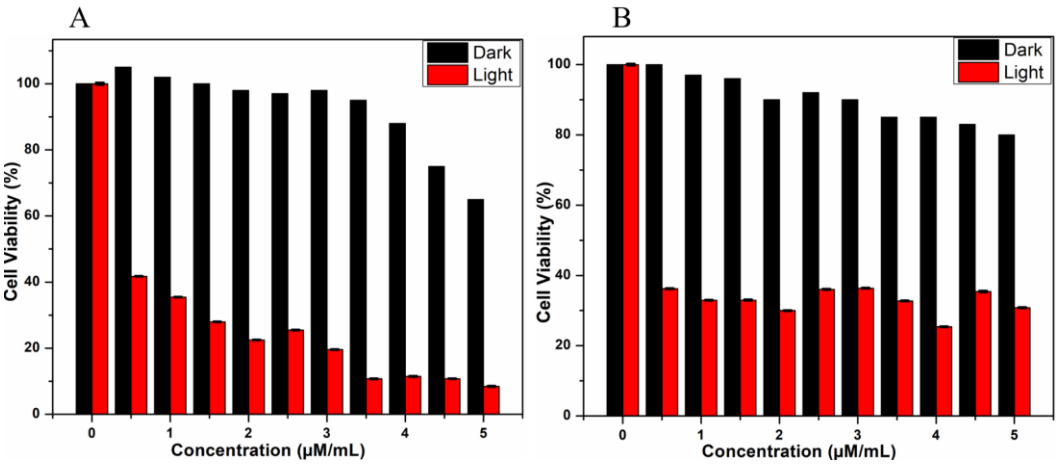

Figure 3.13. (A) TPAV-CM-Py-Me: cell viability results under light and dark (B) TPAV-CM-Py: cell viability results under light and dark

3.6.2. Confocal Results of live Cell Imaging

Confocal laser scanning microscopy (CLSM) was used for AIEgens cell imaging applications. By incubating MCF and MDA-MB-231 cancer cells with both AIEgens (10 μM/mL) for 30 minutes, intense green, fluorescent signals were observed from the cell plasma membrane under confocal microscope (Figure 3.14 B and Figure 3.15 B). To confirm their precise cellular locations/distribution, a co-localization experiment was also performed with a commercial cell membrane staining dye (DiD), nucleus staining dye (Hoechst 33342) and the results are shown in Figures 3.14 (A and C) and 3.15 (A and C), respectively. Both AIEgens overlapped well with DiD, as shown in Figure 3.14 (D) and 3.15 (D), which confirms that our synthesized AIEgens can stain the plasma membrane of MCF-7 cancer cell line. In Figure 3.14 (C) a little blue fluorescence is also observed at the PM of MCF-7 cells, which might be due to the excitation of TPAV-CM-M-Py by the blue channel, owing to its broad absorption range between 360 nm-500 nm (Figure 3.8 A). In addition, DiD also entered the cell to some extent, which is due to the poor PM specificity of DiD.

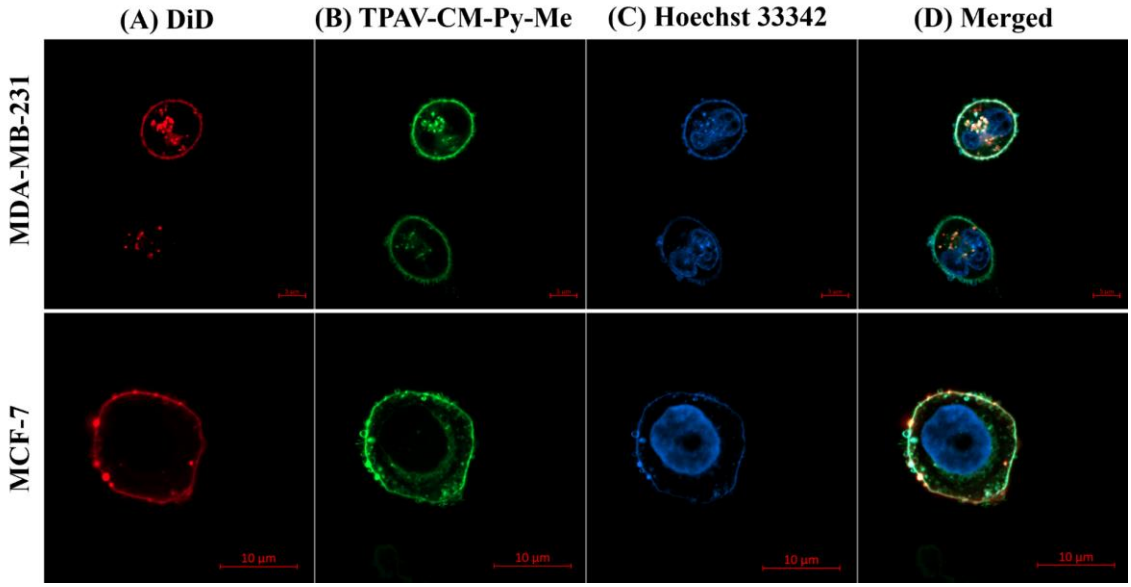

Figure 3.14. TPAV-CM-Py-Me: Live cancer cell analysis

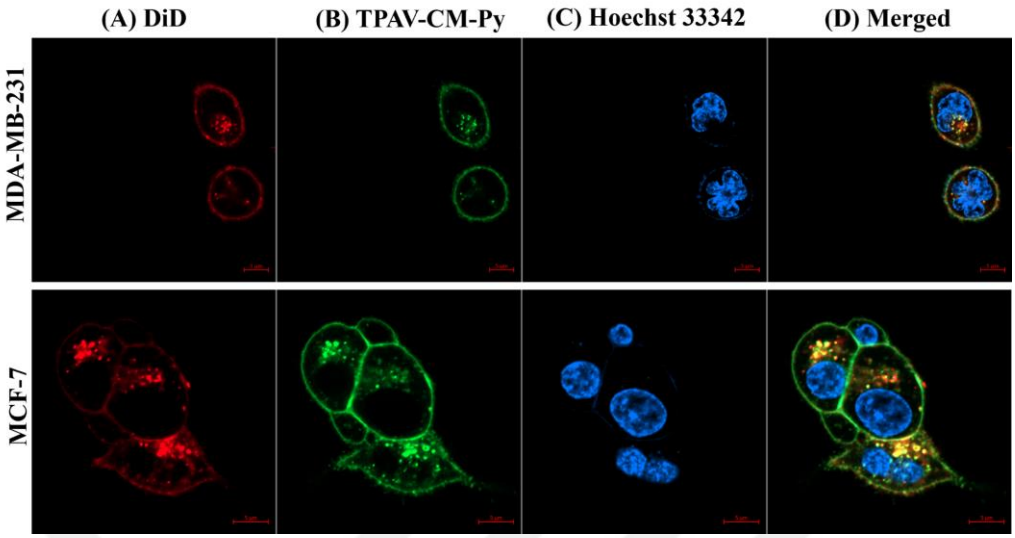

Figure 3.15. TPAV-CM-Py: Live cancer cell analysis

3.7. ROS Generation

The ability of TPAV-CM-Py-Me and TPAV-CM-Py to generate intracellular ROS in MCF-7 was investigated. The experimental section provides detailed procedures for ROS analysis for both designed PSs. Results indicated intracellular ROS generation of TPAV-CM-Py-Me and TPAV-CM-Py by using different concentration (10 µM/mL and 20 µM/mL), as shown in **Figure 3.16.**

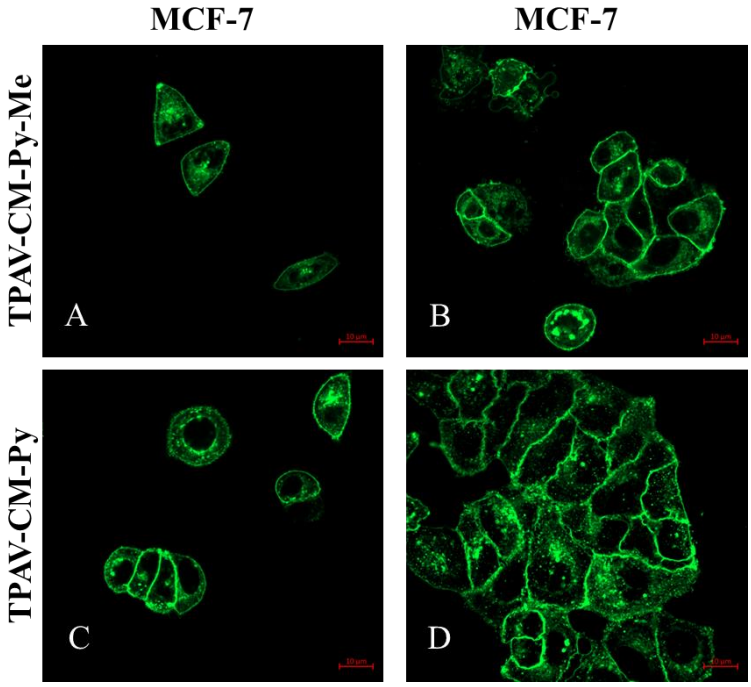

Figure 3.16. TPAVV-CM-Py-Me: (A) 10 µM/mL (B) 20 µM/mL, TPAV-CM-Py: (C) 10 µM/mL (D) 20 µM/mL

CHAPTER 4

CONCLUSION AND SUGGESTIONS

4.1. Conclusion

Organic fluorescent molecules play an important role in biomedical science, particularly biosensing, imaging, and theranostics. Inspired by the widespread use of organic fluorescent molecules as PSs, two novel coumarin-based fluorescent molecules, TPAV-CM-Py-Me and TPAV-CM-Py were synthesized. TPAV-CM-Py-Me and TPAV-CM-Py were designed and synthesized successfully by C-C cross-coupling reaction using the above-mentioned protocol (Scheme 2.1-2.4). Characterization of these synthesized AIE-PSs was also elucidated by NMR and HRMS. First, to observe the photophysical properties of these synthesized AIE-PSs, UV-Vis spectroscopy and fluorescence spectrophotometry analyses were performed. Results revealed that the maximum absorption and emission peaks exhibited in the visible region. TPAV-CM-Py-Me exhibited maximum absorption at 434 nm and fluorescence emission at 640 nm, while TPAV-CM-Py showed maximum absorption at 442 nm and fluorescence emission at 553 nm.

Aggregation induced emission properties of TPAV-CM-Py- Me and TPAV-CM-Py were also observed. Both compounds demonstrated AIE properties in DMSO/toluene mixtures, with TPAV-CM-Py-Me showing maximum fluorescence at 99% toluene fraction and TPAV-CM-Py at 90% toluene fraction. TPAV-CM-Py-Me and TPAV-CM-Py exhibited Stokes shifts of approximately 212 nm and 110 nm, respectively, indicating their potential for biomedical applications due to reduced self-quenching in aggregated states. To confirm the nano size of these AIE-PSs aggregates, DLS analysis was performed, which revealed that TPAV-CM-Py-Me had an aggregation size range of 90-110 nm, whereas

TPAV-CM-Py exhibited a broader size distribution ranging from 10 nm to 160 nm. SEM and STEM analyses confirmed the round shape morphology and nano-scale aggregation round 100 nm of both AIE-PSs.

Under white light irradiation, both AIEgens effectively generated ROS, with TPAV-CM-Py-Me decomposing ABDA in 120 sec and TPAV-CM-Py in 60 sec. After observing the ROS generation properties of synthesized TPAV-CM-Py-Me and TPAV-CM-Py in water, their interaction with mammalian and cancer cells was also studied. CLSM confirmed strong fluorescent signals from the cell plasma membrane, indicating successful cell staining. Furthermore, cell imaging and cytotoxicity assays demonstrated that both TPAV-CM-Py-Me and TPAV-CM-Py exhibited negligible cytotoxicity in the absence of light and significant phototoxicity under light exposure. The intracellular ROS generation was investigated via confocal microscopy using DCFH-DA, and it was found that designed molecules generated intracellular ROS under white light irradiation. Both molecules have a strong affinity for mammalian cells and can easily stain the plasma membrane. Inspired by the high ROS generation and strong affinity toward mammalian cells, they were used against breast cancer cells (MCF-7), and it was found that both AIEgens can kill the cancer cells under white light irradiation. Inspired by their effective use against cancer cells, the designed molecules may find potential practical applications in the photodynamic treatment of cancer.

4.2. Suggestions

These findings suggest that coumarin-based TPAV-CM-Py-Me and TPAV-CM-Py are excellent PSs for advanced cancer treatment by using PDT. To fully realize their therapeutic potential, further studies should focus on enhancing their photodynamic efficiency by differently designing coumarin cores and exploring their potential in in vivo models (mouse modeling).

REFERENCES

1. G. Gunaydin, M. E. Gedik, and S. Ayan, 2021. “PDT for the Treatment and Diagnosis of Cancer–A Review of the Current Clinical Status,” **Frontiers in Chemistry,** vol. 9.

2. S. Kwiatkowski *et al.*, 2018. “PDT – mechanisms, photosensitizers and combinations,” **Biomedicine and Pharmacotherapy, vol. 106**. Elsevier Masson SAS, pp. 1098–1107.

3. M. del P. S. Idelchik, U. Begley, T. J. Begley, and J. A. Melendez, 2017. “Mitochondrial ROS control of cancer,” **Seminars in Cancer Biology, vol. 47**. Academic Press, pp. 57–66.

4. B. Ji, M. Wei, and B. Yang, 2022. “Recent advances in nanomedicines for PDT (PDT)-driven cancer immunotherapy,” **Theranostics, vol. 12**, no. 1. Ivyspring International Publisher, pp. 434–458.

5. D. Sharma, V. Dhayalan, C. Manikandan, and R. Dandela, “Chapter Recent Methods for Synthesis of Coumarin Derivatives and Their New Applications.” [Online]. Available: **www.intechopen.com**

6. M. Lan, S. Zhao, W. Liu, C. S. Lee, W. Zhang, and P. Wang, 2019. “Photosensitizers for PDT,” **Advanced Healthcare Materials, vol. 8**, no. 13. Wiley-VCH Verlag, Jul. 11.

7. R. Wei *et al.*, 2021. “Bioorthogonal Pretargeting Strategy for Anchoring Activatable Photosensitizers on Plasma Membranes for Effective PDT,” **ACS Appl Mater Interfaces, vol. 13**, no. 12, pp. 14004–14014.

8. Q. Xiao *et al.*, 2020. “Pyridine-embedded phenothiazinium dyes as lysosome-targeted photosensitizers for highly efficient photodynamic antitumor therapy,” **J Med Chem, vol. 63**, no. 9, pp. 4896–4907.

9. A. Bouhaoui *et al.*, 2021. “Synthesis and Biological Properties of Coumarin Derivatives. A Review,” **Chemistry Select, vol. 6**, no. 24. John Wiley and Sons Inc, pp. 5848–5870.

10. A. López-Magano *et al.*, 2023. “Recent Advances in the Use of Covalent Organic Frameworks as Heterogenous Photocatalysts in Organic Synthesis,” **Advanced Materials, vol. 35**, no. 24. John Wiley and Sons Inc, Jun. 15.

11. Y. Uruma *et al.*, 2017. “Design, synthesis, and biological evaluation of a highly water-soluble psoralen-based photosensitizer,” **Bioorg Med Chem, vol. 25**, no. 8, pp. 2372–2377.

12. L. Beverina *et al.*, 2008b “Assessment of water-soluble π-extended squaraines as one- and two-photon singlet oxygen photosensitizers: Design, synthesis, and characterization,” **J Am Chem Soc, vol. 130**, no. 6, pp. 1894–1902.

13. K. Santhosh, S. Ganesan, and S. Balamurugan, 2021. “Novel indole-based photosensitizers coupled with PEG-HEC quasi-solid-state electrolyte to improve energy conversion and stability of organic dyes based-dye sensitized solar cells,” **Electrochim Acta, vol. 389**.

14. J. Chen *et al.*, 2020. “Blood distribution and plasma protein binding of Photocyanine: a promising phthalocyanine photosensitizer inphase Ⅱ clinical trials,” **European Journal of Pharmaceutical Sciences, vol. 153**.

15. L. Huang, X. Cui, B. Therrien, and J. Zhao, 2013. “Energy-funneling-based broadband visible-light-absorbing Bodipy-C 60 triads and tetrads as dual functional heavy-atom-free organic triplet photosensitizers for photocatalytic organic reactions,” **Chemistry - A European Journal, vol. 19**, no. 51, pp. 17472–17482.

16. Y. Ma, X. Li, A. Li, P. Yang, C. Zhang, and B. Tang, 2017. “ H 2 S-Activable MOF Nanoparticle Photosensitizer for Effective PDT against Cancer with Controllable Singlet-Oxygen Release ,” **Angewandte Chemie, vol. 129**, no. 44, pp. 13940–13944.

17. F. L. Mi *et al.*, 2017. “Self-Targeting, Immune Transparent Plasma Protein Coated Nanocomplex for Noninvasive Photothermal Anticancer Therapy,” **Adv Healthc Mater, vol. 6**, no. 14.

18. T. Liu *et al.*, 2017. “Triazine-based covalent organic frameworks for photodynamic inactivation of bacteria as type-II photosensitizers,” **J Photochem Photobiol B, vol. 175**, pp. 156–162.

19. J. Mo, N. P. Mai Le, and R. Priefer, 2021. “Evaluating the mechanisms of action and subcellular localization of ruthenium(II)-based photosensitizers,” **European Journal of Medicinal Chemistry, vol. 225**. Elsevier Masson s.r.l.,.

20. N. Mauro, C. Scialabba, S. Agnello, G. Cavallaro, and G. Giammona, “Folic acid-functionalized graphene oxide nanosheets via plasma etching as a platform to combine NIR anticancer phototherapy and targeted drug delivery,” **Materials Science and Engineering C, vol. 107**.

21. I. S. Mfouo-Tynga, L. D. Dias, N. M. Inada, and C. Kurachi, 2020. “Features of third generation photosensitizers used in anticancer PDT: Review,” **Photodiagnosis and PDT, vol. 34**. Elsevier B.V., Jun. 01.

22. J. Ingle and S. Basu, 2023. “Mitochondria Targeted AIE Probes for Cancer Phototherapy,” **ACS Omega, vol. 8**, no. 10. American Chemical Society, pp. 8925–8935.

23. Z. Zhuang *et al.*, 2020. “Type i photosensitizers based on phosphindole oxide for photodynamic therapy: Apoptosis and autophagy induced by endoplasmic reticulum stress,” **Chem Sci, vol. 11**, no. 13, pp. 3405–3417.

24. H. S. Hwang, H. Shin, J. Han, and K. Na, 2018. “Combination of photodynamic therapy (PDT) and anti-tumor immunity in cancer therapy,” **Journal of Pharmaceutical Investigation, vol. 48**, no. 2. Springer Netherlands, pp. 143–151.

25. H. Zhao *et al.*, 2023. “An AIE probe for long-term plasma membrane imaging and membrane-targeted photodynamic therapy,” **Chinese Chemical Letters, vol. 34**, no. 4.

26. J. Kim, O. A. Santos, and J. H. Park, 2014. “Selective photosensitizer delivery into plasma membrane for effective photodynamic therapy,” **Journal of Controlled Release, vol. 191**, pp. 98–104.

27. P. Agostinis *et al.*, 2011. “Photodynamic therapy of cancer: An update,” **CA Cancer J Clin, vol. 61**, no. 4, pp. 250–281.

28. R. Bhole, C. Bonde, P. Kadam, and R. Wavwale, 2021. “A comprehensive review on photodynamic therapy (PDT) and photothermal therapy (PTT) for cancer treatment,” **Turk Onkoloji Dergisi, vol. 36**, no. 1. Istanbul Tip Fakultesi, pp. 125–132.

29. J. O. Yoo and K. S. Ha, 2012. “New Insights into the Mechanisms for Photodynamic Therapy-Induced Cancer Cell Death,” **in International Review of Cell and Molecular Biology, vol. 295**, Elsevier Inc., 2012, pp. 139–174..

30. S. Kwon *et al.*, 2018. “Mitochondria-targeting indolizino [3,2-c]quinolines as novel class of photosensitizers for photodynamic anticancer activity,” **Eur J Med Chem, vol. 148,** pp. 116–127.

31. L. Karami-Gadallo, M. Ghoranneviss, L. Ataie-Fashtami, M. Pouladian, and D. Sardari, 2017. “Enhancement of cancerous cells treatment by applying cold atmospheric plasma and photo dynamic therapy simultaneously,” **Clin Plasma Med, vol. 7–8**, pp. 46–51.

32. H. R. Jia, Y. X. Zhu, K. F. Xu, X. Liu, and F. G. Wu, 2018. “Plasma membrane-anchorable photosensitizing nanomicelles for lipid raft-responsive and light-controllable intracellular drug delivery,” **Journal of Controlled Release, vol. 286,** pp. 103–113.

33. A. Schlachter, P. Asselin, and P. D. Harvey, 2021. “Porphyrin-Containing MOFs and COFs as Heterogeneous Photosensitizers for Singlet Oxygen-Based Antimicrobial Nanodevices,” **ACS Applied Materials and Interfaces, vol. 13**, no. 23. American Chemical Society, pp. 26651–26672.

34. N. Zhang, K. Mei, P. Guan, X. Hu, and Y. Zhao, 2020. “Protein-Based Artificial Nanosystems in Cancer Therapy,” **Small, vol. 16**, no. 23. Wiley-VCH Verlag, Jun. 01.

35. V. D. Turubanova *et al.*, 2021. “Novel porphyrazine-based photodynamic anti-cancer therapy induces immunogenic cell death,” **Sci Rep, vol. 11**, no. 1, Dec. 2021.

36. S. A. Badawy, E. Abdel-Latif, A. A. Fadda, and M. R. Elmorsy, 2022. “Synthesis of innovative triphenylamine-functionalized organic photosensitizers outperformed the benchmark dye N719 for high-efficiency dye-sensitized solar cells,” **Sci Rep, vol. 12**, no. 1.

37. Y. Y. Ling *et al.*, 2022. “Self-Amplifying Iridium(III) Photosensitizer for Ferroptosis-Mediated Immunotherapy Against Transferrin Receptor-Overexpressing Cancer,” **Small, vol. 18**, no. 49.

38. Y. Xu *et al.*, “Long wavelength-emissive Ru(II) metallacycle-based photosensitizer assisting in vivo bacterial diagnosis and antibacterial treatment”, doi: 10.1073/pnas.

39. K. Xiong, F. Wei, Y. Chen, L. Ji, and H. Chao, 2023. “Recent Progress in Photodynamic Immunotherapy with Metal-Based Photosensitizers,” **Small Methods, vol. 7**, no. 5. John Wiley and Sons Inc, May 19.

40. M. Machacek *et al.*, 2015. “Far-red-absorbing cationic phthalocyanine photosensitizers: Synthesis and evaluation of the photodynamic anticancer activity and the mode of cell death induction,” **J Med Chem, vol. 58**, no. 4, pp. 1736–1749.

41. L. Li *et al.*, 2018. “Photosensitizer-Encapsulated Ferritins Mediate Photodynamic Therapy against Cancer-Associated Fibroblasts and Improve Tumor Accumulation of Nanoparticles,” **Mol Pharm, vol. 15**, no. 8, pp. 3595–3599, Aug. 2018.

42. W. Q. Liu *et al.*, 2017. “Visible Light Promoted Synthesis of Indoles by Single Photosensitizer under Aerobic Conditions,” **Org Lett, vol. 19**, no. 12, pp. 3251–3254, Jun. 2017.

43. G. Yu *et al.,* 2019. “Host−guest complexation-mediated codelivery of anticancer drug and photosensitizer for cancer photochemotherapy,” **Proc Natl Acad Sci U S A, vol. 116**, no. 14, pp. 6618–6623.

44. B. Pucelik, L. G. Arnaut, and J. M. Dąbrowski, 2020. “Lipophilicity of bacteriochlorin-based photosensitizers as a determinant for pdt optimization through the modulation of the inflammatory mediators,” **J Clin Med, vol. 9**, no. 1,.

45. B. Pucelik, R. Paczyński, G. Dubin, M. M. Pereira, L. G. Arnaut, and J. M. Dąbrowski, 2017. “Properties of halogenated and sulfonated porphyrins relevant for the selection of photosensitizers in anticancer and antimicrobial therapies,” **PLoS One, vol. 12**, no. 10.

46. X. Feng *et al.,* 2018. “Synthesis, Characterization, and Biological Evaluation of a Porphyrin-Based Photosensitizer and Its Isomer for Effective Photodynamic Therapy against Breast Cancer,” **J Med Chem, vol. 61**, no. 16, pp. 7189–7201,.

47. H. Guo *et al.,* 2020. “Efficient Photooxidation of Sulfides with Amidated Alloxazines as Heavy-atom-free Photosensitizers,” **ACS Omega, vol. 5**, no. 18, pp. 10586–10595.

48. C. A. Gonzalez-Flores *et al.*, 2022. “Influence of Redox Couple on the Performance of ZnO Dye Solar Cells and Minimodules with Benzothiadiazole-Based Photosensitizers,” **ACS Appl Energy Mater, vol. 5**, no. 11, pp. 14092–14106.

49. I. Echevarría, M. Vaquero, B. R. Manzano, F. A. Jalón, R. Quesada, and G. Espino, 2022. “Photocatalytic Aerobic Dehydrogenation of N-Heterocycles with Ir(III) Photosensitizers Bearing the 2(2′-Pyridyl)benzimidazole Scaffold,” **Inorg Chem, vol. 61**, no. 16, pp. 6193–6208.

50. M. Ouyang, L. Zeng, K. Qiu, Y. Chen, L. Ji, and H. Chao, 2017. “Cyclometalated IrIII Complexes as Mitochondria-Targeted Photodynamic Anticancer Agents,” **Eur J Inorg Chem, vol. 2017**, no. 12, pp. 1764–1771.

51. P. Konda *et al.*, 2021. “Discovery of immunogenic cell death-inducing ruthenium-based photosensitizers for anticancer photodynamic therapy,” **Oncoimmunology, vol. 10**, no. 1.

52. X. Feng, Y. Pi, Y. Song, Z. Xu, Z. Li, and W. Lin, 2021. “Integration of Earth-Abundant Photosensitizers and Catalysts in Metal-Organic Frameworks Enhances Photocatalytic Aerobic Oxidation,” **ACS Catal, vol. 11**, no. 3, pp. 1024–1032.

53. J. Cheng *et al.*, 2019. “Simple and Multifunctional Natural Self-Assembled Sterols with Anticancer Activity-Mediated Supramolecular Photosensitizers for Enhanced Antitumor Photodynamic Therapy,” **ACS Appl Mater Interfaces, vol. 11**, no. 33, pp. 29498–29511.

54. P. Y. Ho *et al.*, “Panchromatic Sensitization with ZnII Porphyrin-Based Photosensitizers for Light-Driven Hydrogen Production,” **ChemSusChem, vol. 11**, no. 15, pp. 2517–2528.

55. A. Merabti *et al.*, 2024. “Thiochromenocarbazole imide-based photosensitizers decorated with carbonic anhydrase inhibitors for the targeted treatment of hypoxic tumours,” **Mater Adv,** 2024.

56. S. U. Khan *et al.*, 2020. “Photoelectrochemistry for Measuring the Photocatalytic Activity of Soluble Photosensitizers,” **ChemPhotoChem, vol. 4**, no. 4, pp. 300–306.

57. M. Wu *et al.*, 2021. “Activation of Pyroptosis by Membrane-Anchoring AIE Photosensitizer Design: New Prospect for Photodynamic Cancer Cell Ablation,” **Angewandte Chemie - International Edition, vol. 60**, no. 16, pp. 9093–9098.

58. M. Y. Wu *et al.*, 2023. “From plasma membrane to mitochondria: Time-dependent photodynamic antibacterial and anticancer therapy with a near-infrared AIE-active photosensitizer,” **Chemical Engineering Journal, vol. 454**,.

59. J. Zhao *et al.*, 2023. “Realizing Near-Infrared (NIR)-Triggered Type-I PDT and PTT by Maximizing the Electronic Exchange Energy of Perylene Diimide-Based Photosensitizers,” **ACS Mater Lett, vol. 5**, no. 6, pp. 1752–1759.

60. V. F. Otvagin, N. S. Kuzmina, E. S. Kudriashova, A. V. Nyuchev, A. E. Gavryushin, and A. Y. Fedorov, 2022. “Conjugates of Porphyrinoid-Based Photosensitizers with Cytotoxic Drugs: Current Progress and Future Directions toward Selective Photodynamic Therapy,” **Journal of Medicinal Chemistry, vol. 65**, no. 3. American Chemical Society, pp. 1695–1734, Feb. 10.

61. S. H. Voon *et al.*, 2014. “In vivo studies of nanostructure-based photosensitizers for photodynamic cancer therapy,” **Small, vol. 10**, no. 24, pp. 4993–5013.

62. A. C. Jung, F. Moinard-Butot, C. Thibaudeau, G. Gasser, and C. Gaiddon, 2021. “Antitumor immune response triggered by metal-based photosensitizers for photodynamic therapy: Where are we?,” **Pharmaceutics, vol. 13**, no. 11. MDPI, Nov. 01.

63. J. Liu, L. Lu, D. Wood, and S. Lin, 2020. “New Redox Strategies in Organic Synthesis by Means of Electrochemistry and Photochemistry,” **ACS Cent Sci, vol. 6**, no. 8, pp. 1317–1340.

64. R. Pérez-Ruiz, 2022. “Photon Upconversion Systems Based on Triplet–Triplet Annihilation as Photosensitizers for Chemical Transformations,” **Topics in Current Chemistry, vol. 380**, no. 4. Springer Science and Business Media Deutschland GmbH, Jul. 01, 2022.

65. Y. Zhang, Y. K. Cheung, D. K. P. Ng, and W. P. Fong, “Immunogenic necroptosis in the anti-tumor photodynamic action of BAM-SiPc, a silicon(IV) phthalocyanine-based photosensitizer,” **Cancer Immunology, Immunotherapy, vol. 70**, no. 2, pp. 485–495.

66. X. T. Yu, S. Y. Sui, Y. X. He, C. H. Yu, and Q. Peng, 2022. “Nanomaterials-based photosensitizers and delivery systems for photodynamic cancer therapy,” Biomaterials Advances, vol. 135. Elsevier Ltd, Apr. 01, 2022.

67. A. Citarella, S. Vittorio, C. Dank, and L. Ielo, 2024. “Syntheses, reactivity, and biological applications of coumarins,” **Frontiers in Chemistry, vol. 12**. Frontiers Media SA.

68. A. Shaabani, R. Ghadari, A. Rahmati, and A. H. Rezayan, 2009. “Tetramethylguanidinium Trifluoroacetate Ionic Liquid,”.

69. S. H. Hassanpour and M. Dehghani, 2017. “Review of cancer from perspective of molecular,” **Journal of Cancer Research and Practice, vol. 4**, no. 4, pp. 127–129.

70. H. Cheng *et al.*, 2019. “Chimeric peptide engineered exosomes for dual-stage light guided plasma membrane and nucleus targeted photodynamic therapy,” **Biomaterials, vol. 211**, pp. 14–24, Aug. 2019.

71. J. H. Shon and T. S. Teets, 2019. “Molecular Photosensitizers in Energy Research and Catalysis: Design Principles and Recent Developments,” **ACS Energy Lett, vol. 4**, no. 2, pp. 558–566.

72. S. P. Luo *et al.*, 2013. “Photocatalytic water reduction with copper-based photosensitizers: A noble-metal-free system,” **Angewandte Chemie - International Edition, vol. 52**, no. 1, pp. 419–423.

73. H. Cheng *et al.*, 2019. “Chimeric peptide nanorods for plasma membrane and nuclear targeted photosensitizer delivery and enhanced photodynamic therapy,” **Appl Mater Today, vol. 16**, pp. 120–131.

74. X. Su *et al.*, 2022. “A Carbonic Anhydrase IX (CAIX)-Anchored Rhenium(I) Photosensitizer Evokes Pyroptosis for Enhanced Anti-Tumor Immunity,” **Angewandte Chemie - International Edition, vol. 61**, no. 8.

75. C. Donohoe, M. O. Senge, L. G. Arnaut, and L. C. Gomes-da-Silva, 2019. “Cell death in photodynamic therapy: From oxidative stress to anti-tumor immunity,” **Biochimica et Biophysica Acta - Reviews on Cancer, vol. 1872**, no. 2.

76. H. Cheng *et al.*, 2019. “Mitochondria and plasma membrane dual-targeted chimeric peptide for single-agent synergistic photodynamic therapy,” **Biomaterials, vol. 188**, pp. 1–11.

77. C. Yi *et al.*, 2020. “Nanoscale ZnO-based photosensitizers for photodynamic therapy,” **Photodiagnosis and Photodynamic Therapy, vol. 30**. Elsevier B.V.

78. H. R. Jia *et al.*, 2017. “Plasma membrane activatable polymeric nanotheranostics with self-enhanced light-triggered photosensitizer cellular influx for photodynamic cancer therapy,” **Journal of Controlled Release, vol. 255**, pp. 231–241.

79. S. Zeng *et al.*, 2022. “Activation of pyroptosis by specific organelle-targeting photodynamic therapy to amplify immunogenic cell death for anti-tumor immunotherapy,” **Bioact Mater, vol. 25**, pp. 580–593.

80. R. Wang, X. Li, and J. Yoon, 2021. “Organelle-Targeted Photosensitizers for Precision Photodynamic Therapy,” **ACS Applied Materials and Interfaces, vol. 13**, no. 17. American Chemical Society, pp. 19543–19571.

81. M. del P. S. Idelchik, U. Begley, T. J. Begley, and J. A. Melendez, 2017. “Mitochondrial ROS control of cancer,” **Seminars in Cancer Biology, vol. 47**. Academic Press, pp. 57–66.

82. T. Xia, Z. Xia, P. Tang, J. Fan, and X. Peng, 2023. “Light-Driven Mitochondrion-to-Nucleus DNA Cascade Fluorescence Imaging and Enhanced Cancer Cell Photoablation,” **J Am Chem Soc**.

83. Y. Tian *et al.*, 2024. “DNA-Targeting Bioactive Photosensitizer for Chemo-Photodynamic Therapy of Malignant Tumor,” **ACS Mater Lett, vol. 6**, no. 3, pp. 969–975.

84. R. R. Allison, G. H. Downie, R. Cuenca, X. H. Hu, C. J. H. Childs, and C. H. Sibata, 2004. “Photosensitizers in clinical PDT,” **Photodiagnosis Photodyn Ther, vol. 1**, no. 1, pp. 27–42.

85. T. Xiong *et al.*, 2024. “Lipid Droplet Targeting Type I Photosensitizer for Ferroptosis via Lipid Peroxidation Accumulation,” **Advanced Materials, vol. 36**, no. 4.

86. Y. Ma *et al.*, 2021. “The AIE-Active Dual-Cationic Molecular Engineering: Synergistic Effect of Dark Toxicity and Phototoxicity for Anticancer Therapy,” **Adv Funct Mater, vol. 31**, no. 49.

ATTACHMENTS

Attachment 1.

Appendix A: ^{1}H NMR

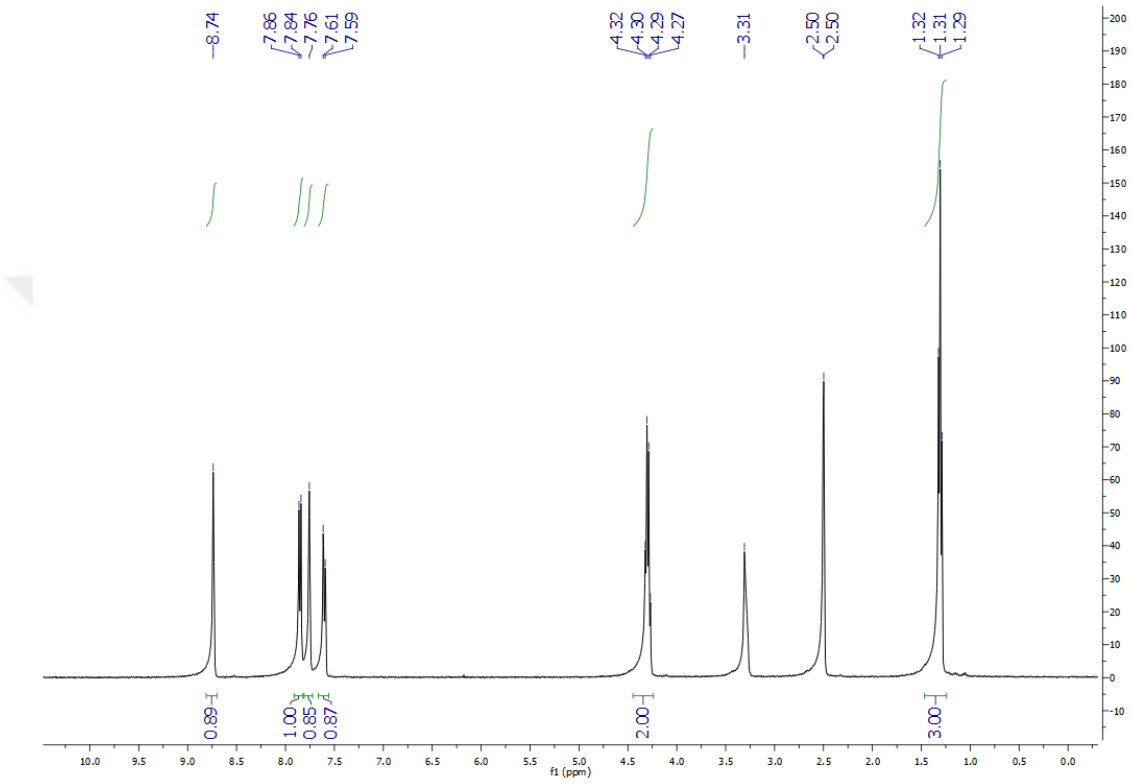

^{1}H-NMR spectrum of Ethyl 7-bromo-2-oxo-2H-chromene-3-carboxylate

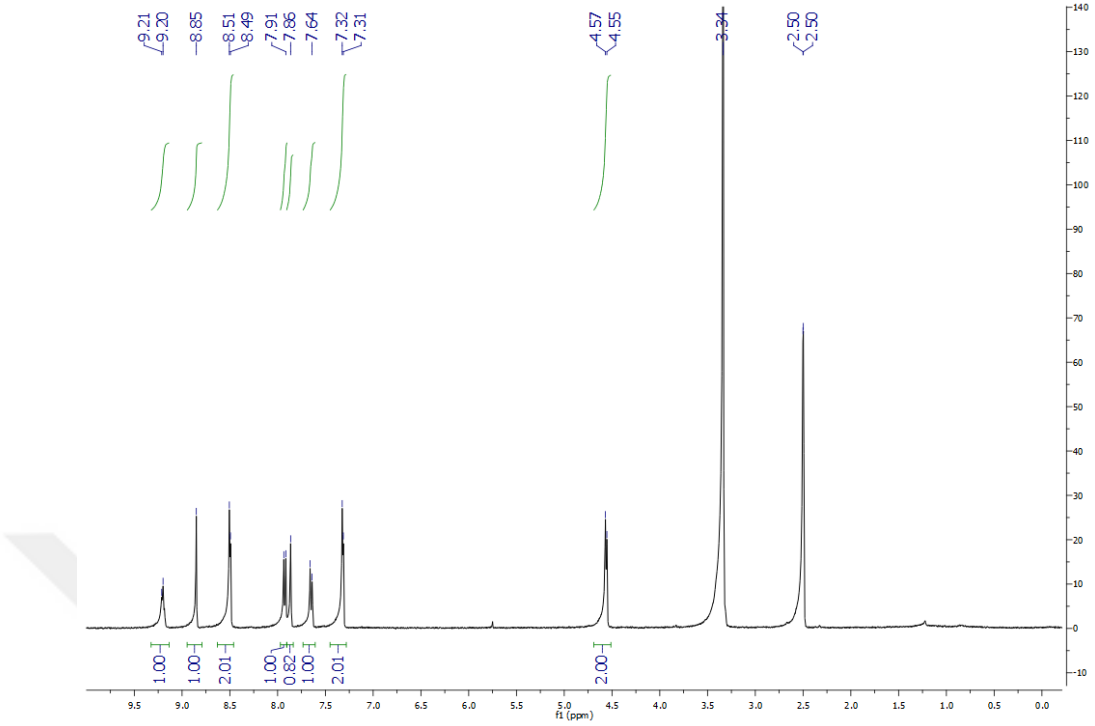

^{1}H-NMR spectrum of 7-methyl-2-oxo-N-(pyridin-4-yl)-2H-chromene-3-carboxamide

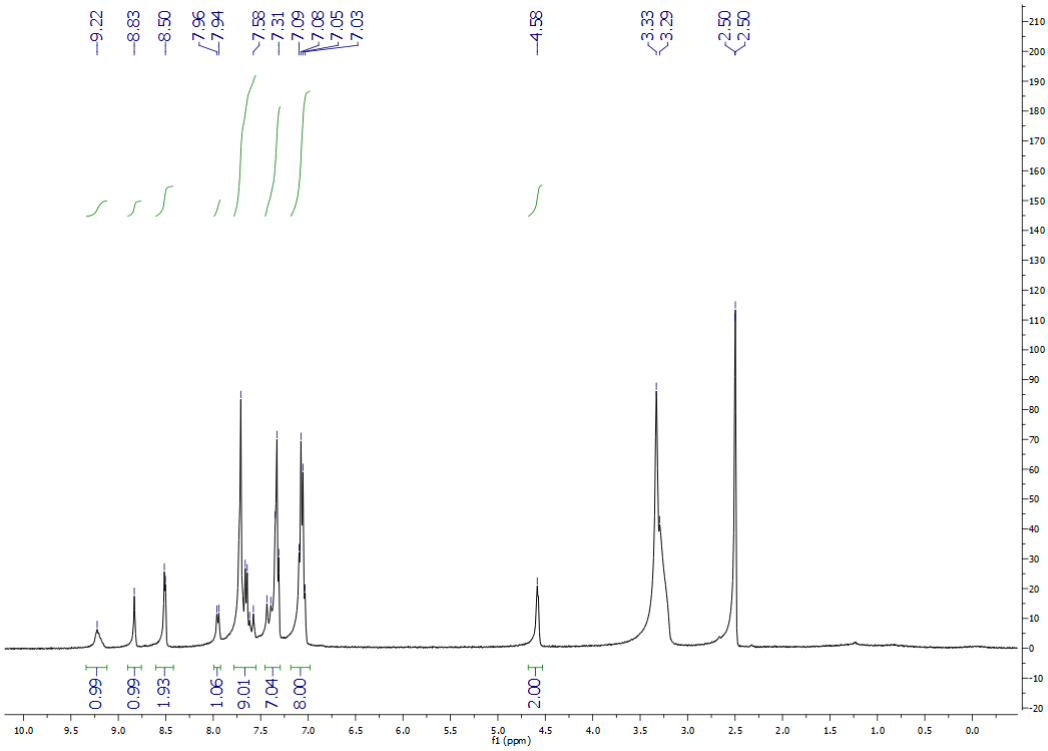

^{1}H-NMR spectrum of (E)-7-(2-(4'-(diphenylamino)-[1,1'-biphenyl]-4-yl)vinyl)-2-oxo-N-(pyridin-4-yl)-2H-chromene-3-carboxamide

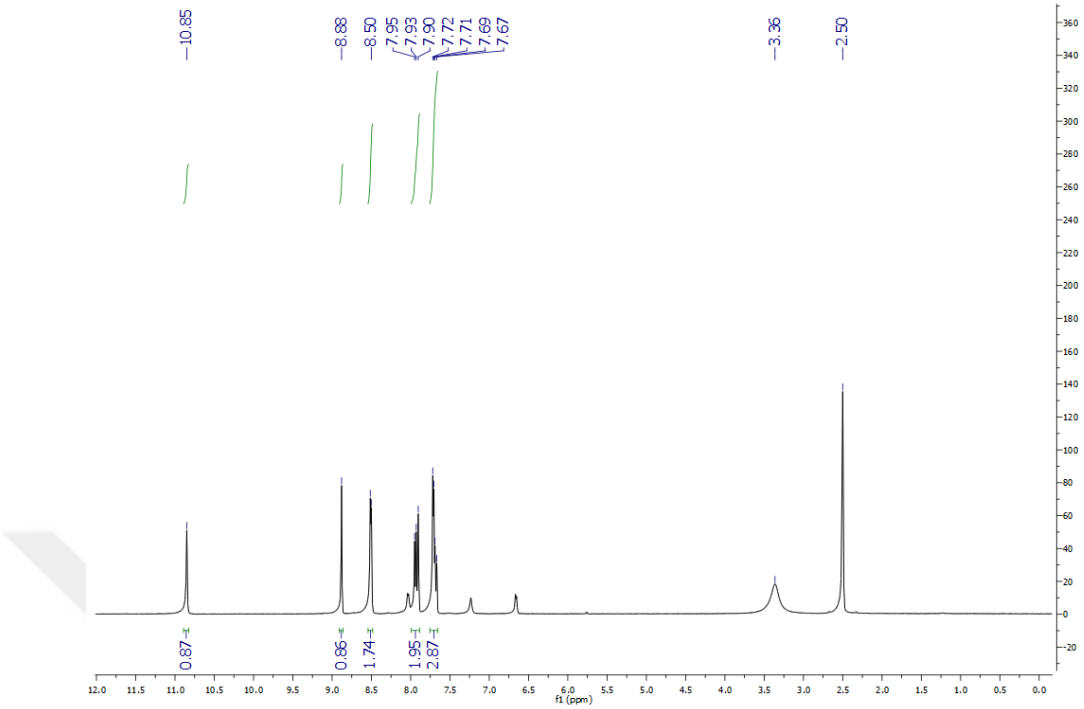

^{1}H-NMR spectrum of 7-bromo-2-oxo-N-(pyridin-4-ylmethyl)-2H-chromene-3-carboxamide

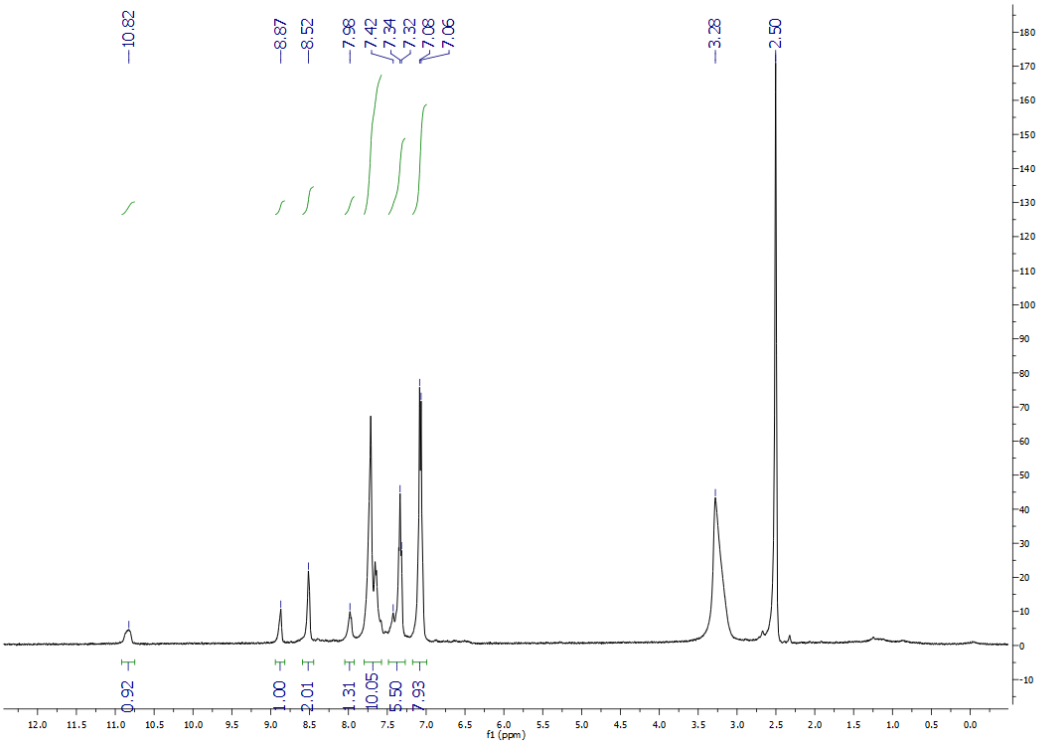

^{1}H-NMR spectrum of (E)-7-(2-(4'-(diphenylamino)-[1,1'-biphenyl]-4-yl)vinyl)-2-oxo-N-(pyridin-4-yl)-2H-chromene-3-carboxamide

CURRICULUM VITAE

PERSONAL INFORMATION

Name and Surname: Abdul Rehman
Nationality: Pakistan (PAK)
Date of Birth - City:
Status:
E-mail:
Adress:

EĞİTİM

Level	Organization	Graduation Date
Bachelor	Government College University Faisalabad	2021
High School	BISE Faisalabad, Pakistan	2017

LANGUAGES

English, Turkish

PUBLICATIONS

1. Rehman, A., & Karacan, I. (2023). PREPARATION AND CHARACTERIZATION OF OXIDIZED VISCOSE RAYON AS ACTIVATED CARBON FIBER PRECURSOR. *ICONTECH INTERNATIONAL JOURNAL*, *7*(1), 1–27. https://doi.org/10.5281/zenodo.7955648

2. Rehman, A. (2024). A Short Overview on Preparation of Different Metal Oxide Nanoparticle by Using Different Techniques. *ICONTECH INTERNATIONAL JOURNAL*, *8*(1). Retrieved https://icontechjournal.com/index.php/iij/article/view/313